POLITECNICO
MILANO 1863

SCUOLA DI INGEGNERIA INDUSTRIALE
E DELL'INFORMAZIONE

Investigation of the Dynamic Models of OpenFAST for the Simulation of Floating Offshore Wind Turbines under Platform Motion

Tesi di Laurea Magistrale in
Energy Engineering - Ingegneria Energetica

Author: **Chiara Morini**

Student ID: 990335
Advisor: Prof. Giacomo Persico
Academic Year: 2022-23

Acknowledgements

Desidero ringraziare tutte le persone che hanno contribuito alla realizzazione di questa tesi.
In primo luogo, ringrazio il mio relatore, il Prof. Persico, per il suo prezioso sostegno e le sue efficaci indicazioni durante tutto il lavoro.
Un ringraziamento importante va a mia madre, che mi ha sostenuta permettendomi di completare questo percorso.
Ringrazio il mio ragazzo che non mi ha mai negato un abbraccio di conforto e una parola di incoraggiamento.
Infine ringrazio la mia migliore amica, con cui ho condiviso i momenti migliori e peggiori della mia esperienza universitaria.

Abstract

The issue of climate change is leading to profound transformations in the energy sector, with wind energy set to play a pivotal role towards a carbon-neutral future. Particularly, the potential of offshore wind energy in Europe has increased the efforts in the research of floating technologies, driving to the development of different platform solutions. However, the inherent unsteadiness of these floating structures requires thorough analyses on the loads exerted on the turbine. Given the limited availability of real-life experimentation of the turbines subjected to the sea movements, tools capable of effectively simulate these conditions are of great importance.

This thesis focuses on the utilization of OpenFAST to investigate its reliability and capability in replicating diverse conditions. The initial segment of this work considers pitch platform motion cases associated to the NREL 5MW baseline turbine. This examination shows the improvements of the code and its validity compared to results obtained with computational fluid dynamics methods. While different models concerning dynamic wake and stall display consistent trends, notable variability in the extreme load points of the motion cycle has suggested a deeper analysis of pertinent parameters. The second part of this study expands the application of OpenFAST by implementing the scaled turbine from the UNAFLOW experimental campaigns in various motion cases. The tool effectively replicates the experimental conditions, yielding results that closely align with anticipated outcomes from the OC6 project. Furthermore, these cases exhibit a close agreement among the models in computing the responses, which are characterized by substantial loads and power oscillations.

Keywords: wind energy; offshore wind turbine; floating platform; scaled turbine; dynamic stall; aerodynamic load; OpenFAST; 5MW; UNAFLOW; OC6

Sommario

Il problema del cambiamento climatico sta conducendo a profonde trasformazioni nel settore energetico, con l'energia eolica destinata a svolgere un ruolo centrale verso un futuro a zero impatto climatico. In particolare, il potenziale dell'energia eolica offshore in Europa ha incrementato gli sforzi nella ricerca della tecnologia, portando allo sviluppo di diverse soluzioni di piattaforme galleggianti. Tuttavia, la non stazionarietà intrinseca di queste strutture richiede analisi approfondite sui carichi esercitati sulla turbina. Date le limitate disponibilità di sperimentazione delle turbine soggette ai movimenti del mare, strumenti capaci di simulare efficacemente queste condizioni rivestono grande importanza.
Questa tesi si concentra sull'utilizzo di OpenFAST per investigare la sua affidabilità e capacità di replicare diverse condizioni. La parte iniziale di questo lavoro esamina casi di moto di pitch della piattaforma, associati alla NREL 5 MW baseline turbine. Questa analisi sottolinea i miglioramenti del codice e la sua validità rispetto ai risultati ottenuti con metodi di fluidodinamica computazionale. Mentre i diversi modelli riguardanti scia instazionaria e stallo dinamico mostrano tendenze similari, una notevole variabilità nei punti di carico estremo del ciclo di moto ha suggerito un'analisi più approfondita dei parametri interessanti. La seconda parte di questo studio espande l'applicazione di OpenFAST attraverso l'implementazione della turbina in scala delle campagne sperimentali UNAFLOW, in vari casi di moto. Lo strumento replica efficacemente le condizioni sperimentali, producendo risultati che si allineano correttamente agli esiti previsti dal progetto OC6. Inoltre, questi casi presentano concordanza tra i modelli nel calcolo delle risposte, le quali sono caratterizzate da sostanziali oscillazioni dei carichi e della potenza.

Parole chiave: energia eolica; turbina eolica offshore; piattaforma galleggiante; turbina in scala; stallo dinamico; carico aerodinamico; OpenFAST; 5MW; UNAFLOW; OC6

Contents

List of Figures

List of Tables

Nomenclature

Symbols

$\underline{e}$	Direction unit vector
$\underline{V}$	Relative airfoil motion vector
$\underline{W}$	Dynamic induction vector
$\underline{W}_{int}$	Intermediate induction vector
$\underline{W}_{qs}$	Quasi-static induction vector
a'	Tangential induction factor
A	Area of the rotor
a	Axial induction factor
c	Chord
C_c	Tangential Coefficient
C_d	Drag Coefficient
C_l	Lift Coefficient
C_n	Normal Coefficient
C_p	Power Coefficient
C_t	Thrust Coefficient
$C_{l,\alpha}$	Lift slope
$C_{l,fs}$	Fully separated lift coefficient
$C_{l,inv}$	Inviscid lift coefficient
C_l^{st}	Static lift coefficient
f	Frequency

f_s^{st}	Steady separation function
P	Power
P_{max}	Maximum theoretical power
Q	Torque
R	Rotor radius
r	Radial position
Re	Reynolds number
T	Thrust
t	Time
T_{rev}	Rotor revolution period
U_o	Freestream/undisturbed wind speed
U_{ac}	Velocity norm at aerodynamic center
x_i	State
z_0	Roughness length

Greek symbols

α	Angle of attack
α_0	Zero lift angle of attack
α_{34}	Angle of attack at 3/4 chord point
Ω	Rotor rotational speed
ω	Pitching rate of the airfoil section
Ω_p	Angular frequency
ϕ	Phase
ρ	Air density
τ	Time constant
Θ	Amplitude
θ_0	Initial position

θ_p	Position

Acronyms

AoA	Angle of Attack
$B-L$	Beddoes-Leishman
$BEMT$	Blade Element Momentum Theory
CFD	Computational Fluid Dynamics
$DBEMT$	Dynamic Blade Element Momentum Theory
DoF	Degree of Freedom
DTU	Technical University of Denmark
EU	European Union
$Ex1$	Experimental campaign 1
$Ex2$	Experimental campaign 2
$FOWT$	Floating Offshore Wind Turbine
GHG	Green House Gases
$HAWT$	Horizontal Axis Wind Turbine
IEA	International Energy Agency
$LCOE$	Levelized Cost Of Electricity
$NREL$	National Renewable Energy Laboratory
$OC6$	Offshore Code Comparison Collaboration, Continued, with Correlation and unCertainty
UA	Unsteady Aerodynamics
$UNAFLOW$	Unsteady Aerodynamics for FLOating Wind

1 | Introduction

Nowadays, climate change is a global issue that can lead, for example, to biodiversity loss, forest fires, decreasing crop yields, and higher temperatures. It is caused by greenhouse gas (GHG) emissions, with carbon dioxide (CO_2) accounting for almost 80% of the volume in 2021. In the European Union (EU), which was the fourth-largest emitter in 2019, after China, the USA and India, the energy sector was responsible for 77% of GHG emissions, stressing the need for a transition from fossil fuel-based plants to renewable sources [12]. To address this problem, the EU released the "Fit for 55" package: a set of proposals with the target of reducing emissions by at least 55% by 2030 and achieving carbon neutrality by 2050. It also contained the objective, for the energy sector, to reach at least 40% of renewable sources in the energy mix by the same year [11].
In this challenge towards sustainability, wind energy is set to play a key role. It currently meets 15% of Europe's electricity demand, with figures exceeding this percentage in nations such as Denmark, Ireland, and Portugal. The International Energy Agency (IEA) also predicts it will be the first power source in Europe by 2027 [25].
Focusing on Italy, wind energy totaled for 11 GW of installed power in 2020, with plants mostly located in the southern regions, which generated 20 TWh during the year. In the future, this resource is estimated to be exploited further by means of new installations, repowering, and offshore wind plants coming in the next years. [10].
Electricity obtained from wind energy produces no CO_2 emissions, it is also useful in remote areas where the grid is weak, especially when combined with batteries and diesel engines. In locations where the wind resource is abundant, the levelized cost of electricity (LCOE) of a wind plant is now competitive with more traditional fossil fuel-fired ones. Efforts to reduce costs focus on the price of the turbines themselves, with land use costs and wind availability also being influential. To optimize annual energy production, it is important to couple information about the wind distribution of the site with the characteristics of the machine. The main drawback of this type of energy is its non-programmable nature, as production depends on the presence of wind, which needs reliable weather forecasts to be effectively predicted. Other issues concern noise and visual impact on the people living close by, also considering the trend of increasing size of the rotors.

Wind turbines work by transforming kinetic energy from the wind into mechanical energy and finally electrical energy through a generator. The maximum theoretical power obtainable with a certain wind speed is thus:

$$P_{max} = \frac{1}{2}\rho A U_0^3 \tag{1.1}$$

where U_0 is the wind speed, ρ is the density and A the area of the rotor. From this equation, the importance of the site available wind speed distribution is stressed, as power increases with its cube. An additional coefficient of power C_p has to be added to equation 1.1, as the wind can't be completely stopped by the turbine, and the theoretical maximum, called the Betz limit, sets $C_{p,max} = 0.593$, with modern turbines reaching $C_p = 0.5$.

Commercial wind turbines rely on lift forces to extract power as it is much more efficient. Therefore, the blades are shaped using specifically optimized airfoil profiles. Moreover, the majority of plants employ horizontal axis wind turbines (HAWT), which are characterized by the blades being connected to a horizontal shaft and the hub placed on top of a tower. The height of the tower contributes to reaching faster winds. Three-bladed configurations are preferred for higher efficiency and less visual disturbance, in combination with an upwind rotor that can be yawed to follow the wind direction by the control system, which is in charge of regulating the power too.

As stated before, energy production by a turbine depends on the wind field of a site, which is characterized by shear, meaning that speed increases with height from the ground. Wind speed at a certain elevation x can be estimated as:

$$\frac{U_0(x)}{U_0(h)} = \frac{ln(x/z_0)}{ln(h/z_0)} \tag{1.2}$$

where h is a fixed height and z_0 is the roughness length, which depends on the ground surface characteristics and corresponds to a minimum of 10^{-4} m over water [14].

This is one of the reasons why offshore wind plants are being built, together with an overall higher wind speed on sea and availability of large, free areas. However, traditional bottom-fixed offshore wind is not viable in waters deeper than 60 m, where 80%, or 4000 GW, of resource potential in Europe is located. For this reason, floating offshore wind turbines (FOWT), which can expand the capacity of the existing offshore industry to new regions, have been investigated in R&D and are now becoming ready for commercialization. As the development of the turbines, electrical parts, and operation and maintenance strategies are overlapped with the bottom-fixed solution, the technology focuses on the

floating substructures. Currently, four main types are being developed: spar buoy, semi-submersible, barge, and tension leg platforms, with the first three being moored to the seabed, while the last one is more firmly connected to the bottom. The first two typologies are also at a technology readiness level appropriate for operation.
Despite their great potential, FOWT projects are still in the early stages and require significant investments and commitment, both from investors and politicians, through incentives and planning. Nonetheless, the IEA suggests a possible FOWT cost reduction of 50% by 2050, due to parallel development with fixed-bottom turbines, larger sizes capable of harnessing the higher wind speeds, increasing their capacity factor, and, finally, reduced costs and risks related to the construction and maintenance of the floating platforms compared to the fixed ones [24].
The FOWT substructures, by not being rigidly fixed to the seafloor, are subjected to significant translational and rotational motions, which affect the system and the loads. Experimental campaigns, such as the Unsteady Aerodynamics for FLOating Wind (UNAFLOW) project, are able to simulate steady and unsteady wind conditions due to the platform degrees of freedom (DoFs). However, when this type of approach is not available, different modeling tools can be utilized for simulating and analyzing FOWTs in these conditions. The objective of the Phase III of the Offshore Code Comparison Collaboration, Continued, with Correlation and unCertainty (OC6) project is to evaluate the accuracy of aerodynamic load predictions under large motions of such tools, among which OpenFAST is taken into consideration [6].
OpenFAST is an open-source simulation tool developed by the National Renewable Energy Laboratory (NREL) for the analysis of a range of wind turbine configurations, both onshore and offshore, coupling modules for the different dynamics of the system.
In the aerodynamics module, OpenFAST contains the possibility of using Blade Element Momentum Theory (BEMT) or Dynamic Blade Element Momentum Theory (DBEMT) calculations. The first method enables the computation of steady loads for different operating conditions, combining the momentum theory with the blade element theory, which considers local phenomena due to the rotor geometry, discretizing the analysis in elements. Nevertheless, the important platform motions FOWTs are exposed to render the real airflow around it unsteady, which calls for dynamic inflow corrections of the BEMT method during the simulation time, which can be further expanded to consider Unsteady Aerodynamics models for dynamic stall, affecting the lift and drag coefficient of the blade profiles [4, 7].
Therefore, this thesis intends to investigate the reliability of the various BEMT methods available in the OpenFAST code for simulating loads due to the DOFs of the substructure of a FOWT. The BEMT, DBEMT, Beddoes-Leishman 4 and 5 states, and the Øye model

will be studied.
In the beginning, the analysis considers the NREL 5MW baseline wind turbine at a wind speed of 11 m/s, pitch motion cases ranging between amplitudes of 1 to 4 degrees and frequencies between 0.1 and 0.025 Hz, including also an extreme pitching of 0.2 Hz. Then, the study moves to the 1:75 scaled turbine of the Technical University of Denmark (DTU) 10MW reference wind turbine used in the UNAFLOW project. First, to define a procedure to implement this new machine in the OpenFAST tool files, next, to replicate the cases of the experimental campaign and the OC6 project, with the aim of comparing simulation results and verifying the quality of the models. These cases comprise two steady conditions at wind speeds of 4.19 and 6.03 m/s, thus, continuing with the first value, unsteady cases obtained by adding platform motions of either surge or pitch. The last simulations regard the verification cases, which were not experimentally obtained and are based on a more extreme surge motion, to recreate the above-rated operation of a turbine with a controller, which actuates blade pitch variations of 1.5 deg of amplitude.

1.1. Thesis Outline

This thesis is structured as follows:

Chapter 2: Literature survey introduces the floating turbine problem and its characteristics, moving to the explanation of the unsteady phenomena of dynamic wake and stall. Finally, a general overview of the OpenFAST tool and its components is given.

Chapter 3: 5MW turbine gives a first overview and describes the implementation of the 5MW baseline turbine, followed by the results of various pitch platform motion cases.

Chapter 4: OC6 turbine begins by describing the scaled turbine of the UNAFLOW experimental campaigns and the OC6 project. Then, the implementation of the turbine in OpenFAST is thoroughly explained. Lastly, the results of the steady and unsteady simulations are analyzed.

Chapter 5: Conclusions and future developments sums up the most relevant results of this thesis and the possible future works on this subject.

2 | Literature survey

2.1. Floating turbine dynamics

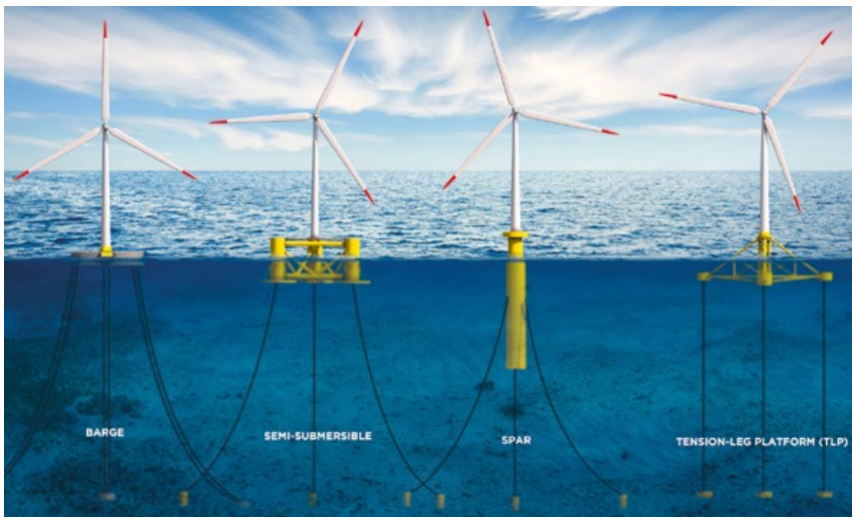

Figure 2.1: Floating platform typologies. Figure from [25]

FOWTs rely on floating platforms similar to the ones presented in Figure 2.1, which are based on different strategies for stability, namely ballast weights, mooring lines, or distributed buoyancy. These technologies derive from the experience of offshore oil rigs; hence, their durability can be demonstrated. However, the challenge lies in the prediction of loads and dynamic responses of the system. In fact, the structures have six main DoFs divided between translational (surge, sway, and heave) and rotational (roll, pitch, and yaw) movements, and their intensity depends on the type of floater and the different loading sources, including the hydrodynamic effects of waves [9].
One example of the real operational offshore conditions of a floating turbine is given by Statoil's "Hywind Demo" demonstration unit: a 2.3 MW turbine mounted on a spar-type substructure and installed off the coast of Norway in 2009.

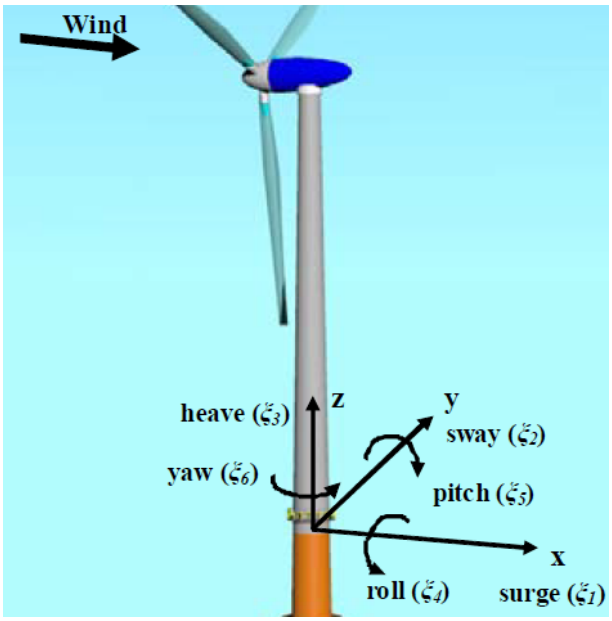

Figure 2.2: FOWT degrees of freedom. Figure from [9]

In the left Figure 2.3, a below-rated wind speed period with a calm sea state is shown, where the oscillations are contained under 0.2 deg. In contrast, the right Figure 2.3 depicts a more extreme situation that pushed the pitch angle of the system up to almost 6 deg, causing shutdown of the turbine when the floater motion controller was deactivated [23].

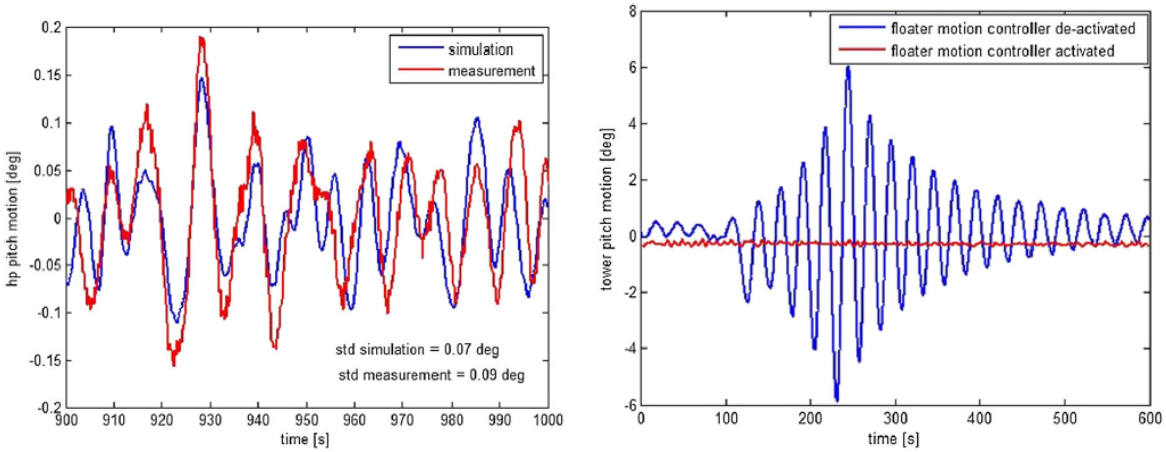

Figure 2.3: Hywind pitch motion response during operation. Taken from [23]

Platform movements of this scale can cause significant variations of the incoming wind experienced by the turbine. Consequently, the wake is affected, as well as the angle of attack (AoA) of each blade.

2.2. Unsteady Aerodynamics

The choice of the modeling approach is based on a trade-off between fidelity and computational efficiency, with respect to the studied phenomena and performance levels. BEMT methods are mid-fidelity approaches based on the more simple and used steady BEMT. The motions described before are one of the factors that render the flow unsteady, so, in those conditions, corrections are introduced to the BEMT models to obtain a DBEMT algorithm.

2.2.1. Dynamic inflow/wake

Baseline BEMT assumes that the wake has an instantaneous reaction to changes in the flow conditions, with quasi-steady induced velocities. However, in reality, wake response has a time delay which is taken into consideration by a dynamic inflow or dynamic wake model in the DBEMT [6].
The time scales of the phenomenon are related to the convection velocity of the vorticity. Following a loading change, the new vorticity values emitted into the wake progressively propagate downstream, substituting the old values, resulting in a gradual change of the induced velocities, too. Additionally, the delay at the tip is shorter than at the root. The dynamic inflow models generally introduce an exponential decay to act as a filter between the current flow configuration and the quasi-static values of baseline BEMT [7].

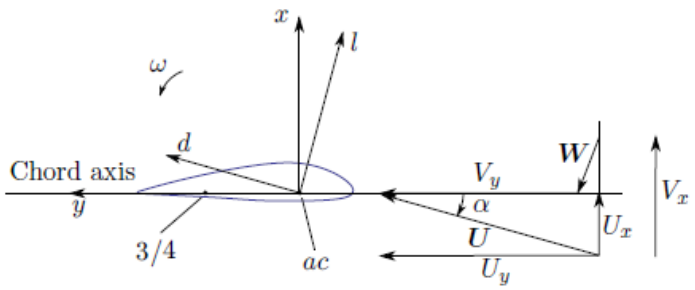

Figure 2.4: Notations for the aerodynamic models. Figure from [8]

The model implemented in OpenFAST, and considered in this work, is the Øye model described by Branlard in [7] and is written using two first-order differential equations:

$$\underline{W}_{qs} + 0.6\,\tau_1\,\underline{\dot{W}}_{qs} = \underline{W}_{int} + \tau_1\,\underline{\dot{W}}_{int}\ , \qquad \underline{W}_{int} = \underline{W} + \tau_2\,\underline{\dot{W}} \tag{2.1}$$

First of all, the "$\cdot$" denotes a time derivative, while the "_" a vector. In equation 2.1:

τ_1 and τ_2 are time constants, $\underline{W}$ is the dynamic induction vector at the rotor (at a given blade position and radial position), $\underline{W}_{qs}$ is the quasi-steady induction, $\underline{W}_{int}$ is an intermediate value coupling the quasi-steady and the dynamic inductions. In a steady solution $\underline{W} = \underline{W}_{qs}$, while in an unsteady step, once the axial and tangential quasi-steady induction coefficients a and a' are computed, the values are found as:

$$\underline{W}_{qs} = -a\, V_x\, \underline{e}_x - a'\, V_y\, \underline{e}_y \tag{2.2}$$

$$\tau_1 = \frac{1.1}{1 - 1.3\, min(\overline{a}, 0.5)}\, \frac{R}{\overline{U}_0}\,, \qquad \tau_2 = \left(0.39 - 0.26\, \frac{r^2}{R^2}\right)\, \tau_1 \tag{2.3}$$

where the symbols: $\underline{V}$ is the vector of the relative motion of the airfoil (wind and elastic), without the induced velocity, R is the rotor radius, r is the radial position, $\overline{U}_0$ is the average wind speed over the rotor, $\overline{a}$ is the average axial induction over the rotor, $\underline{e}_x$ and $\underline{e}_y$ are the unit vectors of the directions as shown in Figure 2.4.
The Equations (2.1) are resolved by using backward differences between the $i-1$ and i successive time steps (separated by Δt), leading to:

$$\underline{H} = W^i_{qs} + 0.6\, \tau_1\, \frac{\underline{W}^i_{qs} - \underline{W}^{i-1}_{qs}}{\Delta t} \tag{2.4}$$

$$\underline{W}^i_{int} = \underline{H} + (\underline{W}^{i-1}_{int} - \underline{H})\, e^{-\frac{\Delta t}{\tau_1}}\,, \qquad \underline{W}^i = \underline{W}^i_{int} + (\underline{W}^{i-1} - \underline{W}^i_{int})\, e^{-\frac{\Delta t}{\tau_2}} \tag{2.5}$$

In Figure 2.5, an example of the implementation in OpenFAST of the dynamic inflow model is visible in a case applied to the 5MW turbine, at constant rotational speed and uniform wind speed: a blade pitch step event suddenly changes the circulation along the blade, however, its propagation delays the realization of a new steady state in the wake [8].

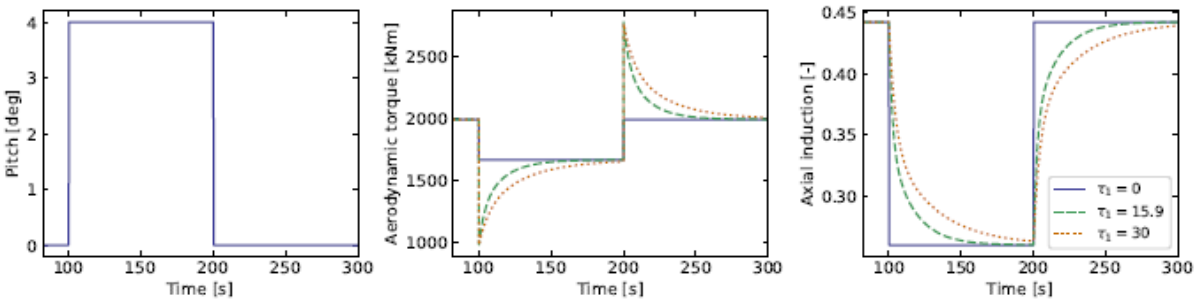

Figure 2.5: Response to a blade pitch step using the dynamic inflow model for different values of τ_1. Taken from [8]

2.2.2. Dynamic stall

The dynamic response of the aerodynamic loads depends on the fluid state in the boundary layer, which can be attached or separated, depending on the past flow and airfoil motion. Dynamic stall models predict the performance of the airfoil under these unsteady conditions, providing a lift coefficient (C_l) - AoA (α) relation based on the time history of α, relying on time constants connected to the time needed for the boundary layer to adapt to configuration changes [7]. Some of the models present in OpenFAST are described in the following sections.

Beddoes-Leishman models

The first described model is a Beddoes-Leishman (B-L) type presented by Hansen, Gaunaa, and Madsen [13] but slightly modified for OpenFAST, as explained by Branlard in [8] and the tool manual [4].
The original B-L model includes the unsteady effects of two-dimensional wake, trailing and leading edge, and compressibility. However, the formulation described next is specifically intended for wind turbines, which have limited maximum tip speeds and use relatively thick airfoils, allowing compressibility effects and leading edge flow separation to be neglected [13].
This 4-states incompressible model relies on parameters obtained from C_l, drag coefficient (C_d), and moment coefficient (C_m). It also uses the zero lift angle of attack (α_0) and the lift slope at that location ($C_{l,\alpha}$) to calculate the steady separation function (f_s^{st}) for the trailing edge and the fully separated lift coefficient ($C_{l,fs}$).

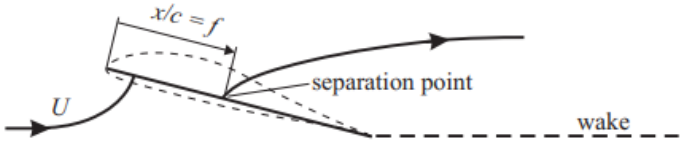

Figure 2.6: Trailing edge separation point defined in the Kirchoff flow past a flat plate. Figure from [13]

f_s^{st} is obtained as function of the AoA from the static lift coefficient (C_l^{st}) on a flat plate

in a potential Kirchhoff flow:

$$Close\ to\ \alpha_0\,,\, f_s^{st} = min\left\{\left[2\sqrt{\frac{C_l^{st}(\alpha)}{C_{l,\alpha}\,(\alpha-\alpha_0)}}-1\right]^2\ 1\right\}\,, \tag{2.6}$$

$$away\ from\ \alpha_0\,,\, f_s^{st} = 0 \tag{2.7}$$

The fully separated lift coefficient is instead obtained from f_s^{st} as:

$$C_{l,fs}(\alpha) = \frac{C_l^{st}(\alpha) - C_{l,\alpha}(\alpha-\alpha_0)\,f_s^{st}(\alpha)}{1-f_s^{st}(\alpha)}\ when\ f_s^{st} \neq 1\,, \tag{2.8}$$

$$C_{l,fs}(\alpha) = \frac{C_l^{st}(\alpha)}{2}\ when\ f_s^{st} = 1 \tag{2.9}$$

while the inviscid (i.e. without separation) lift coefficient is:

$$C_{l,inv} = C_{l,\alpha}(\alpha-\alpha_0) \tag{2.10}$$

Next, the model takes as input the AoA at 3/4 chord point (α_{34}), the velocity norm at the aerodynamic center (U_{ac}) and the pitching rate of the airfoil section (ω). The first point refers originally to the position on the chord axis located 3/4 of the chord behind the leading edge, in OpenFAST it is generalized to a mid-way point between the aerodynamic center and the trailing edge. The aerodynamic center is located where the aerodynamic forces and moment are assumed to act on the airfoil cross-section, usually close to 1/4 of the chord. Moreover, the other involved parameters are:

- $A_1,\ A_2,\ b_1,\ b_2$: characteristic constants of the propagation of the wake vorticity (Wagner constants);
- $T_u = min\left(\frac{c}{2\,U_{ac}(t)},\,50\right)$ (c is the airfoil chord): time for the flow to go over half the airfoil section;
- $T_f = T_{f,0}\,T_u,\ T_p = T_{p,0}\,T_u$: time constants associated with trailing edge stall and boundary layer pressure gradient respectively, derived from other time constants $T_{f,0}$ and $T_{p,0}$;

The four states ($x_1 - x_4$) correspond to two downwash memory terms representing the shed vorticity in the wake in attached flows, a lift coefficient with a time-lag to the attached

lift, and the position of the separation point. The state equations are:

$$\dot{x}_1 = -T_u^{-1}\, b_1\, x_1 + T_u^{-1}\, b_1\, A_1\, \alpha_{34} \tag{2.11}$$
$$\dot{x}_2 = -T_u^{-1}\, b_2\, x_2 + T_u^{-1}\, b_2\, A_2\, \alpha_{34} \tag{2.12}$$
$$\dot{x}_3 = -T_p^{-1}\, x_3 + T_p^{-1}\, C_l^p \tag{2.13}$$
$$\dot{x}_4 = -T_f^{-1}\, x_4 + T_f^{-1}\, f_s^{st}(\alpha_F),\ x_4 \in [0,1] \tag{2.14}$$

with the intermediate variables being an effective angle of attack, the unsteady lift for attached flow, and an equivalent angle of attack for the same quasi-steady lift:

$$\alpha_E(t) = \alpha_{34}(t)\,(1 - A_1 - A_2) + x_1(t) + x_2(t) \tag{2.15}$$
$$C_l^p(t) = C_{l,\alpha}(\alpha_E(t) - \alpha_0) + \pi T_u(t)\,\omega(t) \tag{2.16}$$
$$\alpha_F(t) = \frac{x_3(t)}{C_{l,\alpha}} + \alpha_0 \tag{2.17}$$

The outputs of the model are the unsteady airfoil coefficients, obtained from the states as follows:

$$C_{l,dyn}(t) = C_{l,circ} + \pi\, T_u\, \omega \tag{2.18}$$
$$C_{d,dyn}(t) = C_d(\alpha_E) + [(\alpha_{34} - \alpha_E) + T_u\,\omega]\, C_{l,circ} + [C_d(\alpha_E) - C_d(\alpha 0)]\, \Delta C''_{d,f} \tag{2.19}$$
$$C_{m,dyn}(t) = C_m(\alpha_E) - \frac{\pi}{2}\, T_u\, \omega \tag{2.20}$$

where the intermediate variables come from:

$$C_{l,circ} = x_4(\alpha_E - \alpha_0)\, C_{l,\alpha} + (1 - x_4)\, C_{l,fs}(\alpha_E) \tag{2.21}$$
$$\Delta C''_{d,f} = \frac{\sqrt{f_s^{st}(\alpha_E)} - \sqrt{x_4}}{2} - \frac{f_s^{st}(\alpha_E) - x_4}{4}, \quad x_4 \geq 0 \tag{2.22}$$

For what concerns the other B-L model, the 5-states incompressible one adds a fifth state which represents vortex generation, and instead uses the normal coefficient (C_n) and tangential coefficient (C_c) as main quantities, formulating the separation function as follows:

$$f_s^s(\alpha) = \left[2\, max\left\{\frac{1}{4},\ \sqrt{\frac{C_n^{st}(\alpha) - C_{n,offset}}{C_n^{fullyAttached}(\alpha) - C_{n,offset}}}\right\} - 1\right]^2 \tag{2.23}$$

$$C_{n,offset} = \frac{C_n(\alpha^{lower)} + C_n(\alpha^{upper})}{2} \tag{2.24}$$

with α^{upper} and α^{lower} being the AoA of the upper and lower boundary of fully attached region for the C_n or C_l curve, and $C_n^{fullyAttached}$ is defined as C_n between these two values or as linear functions outside of them.

$$C_n^{fullyAttached}(\alpha) = \begin{cases} C_n(\alpha^{upper}) + C_n^{slope}(\alpha^{upper})(\alpha - \alpha^{upper}) & \alpha > \alpha^{upper} \\ C_n(\alpha) & \alpha^{lower} \leq \alpha \leq \alpha^{upper} \\ C_n(\alpha^{lower}) + C_n^{slope}(\alpha^{lower})(\alpha - \alpha^{lower}) & \alpha < \alpha^{lower} \end{cases} \tag{2.25}$$

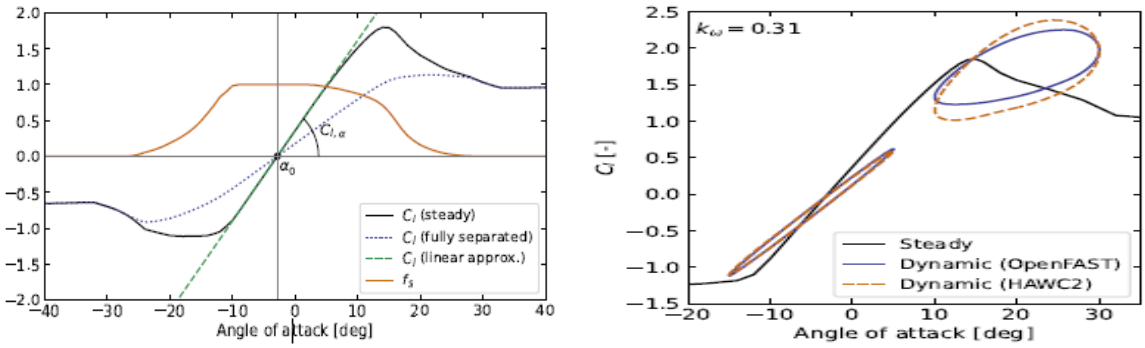

Figure 2.7: For an example airfoil: (left) steady, fully separated, linearly approximated lift coefficient curves and separation function; (right) dynamic airfoil coefficients obtained from a sinusoidal pitching of an airfoil section about its mid chord. Taken from [8]

Øye model

Øye's dynamic stall model [4, 7] is a one-state model which considers trailing edge stall. It computes the aerodynamic data by linear combination of two extreme cases: the fully separated or fully inviscid flow, using its only state $x = f_s$, defined as the unsteady separation function, as a relaxation factor. The first-order, differential, state equation is the following:

$$\dot{f}_s(t) = -\frac{1}{T_f} f_s(t) + \frac{1}{T_f} f_s^{st}(\alpha_{34}(t)) \tag{2.26}$$

it can be noted that f_s reaches f_s^{st} when the system is in steady state.
Finally, the output unsteady lift coefficient is calculated as:

$$C_{l,dyn}(\alpha_{34}, t) = f_s(t)\, C_{l,inv}(\alpha_{34}) + (1 - f_s(t))\, C_{l,fs}(\alpha_{34}) \tag{2.27}$$

2.3. OpenFAST

OpenFAST [16] provides the possibility of simulating individual land-based, fixed-bottom or floating offshore turbines, coupling the different dynamics of the system. The tool has the ability to run nonlinear time-domain simulations in real time for loading analyses and to linearize the unlinear model to enable, for example, controls design.
In this thesis the OpenFAST v3.4.1 version was used.
The mathematical models used for the simulation are implemented in separated modules and then interconnected to solve the global, coupled, dynamic response of the system.
Figure 2.8 shows the various modules and their interconnections.

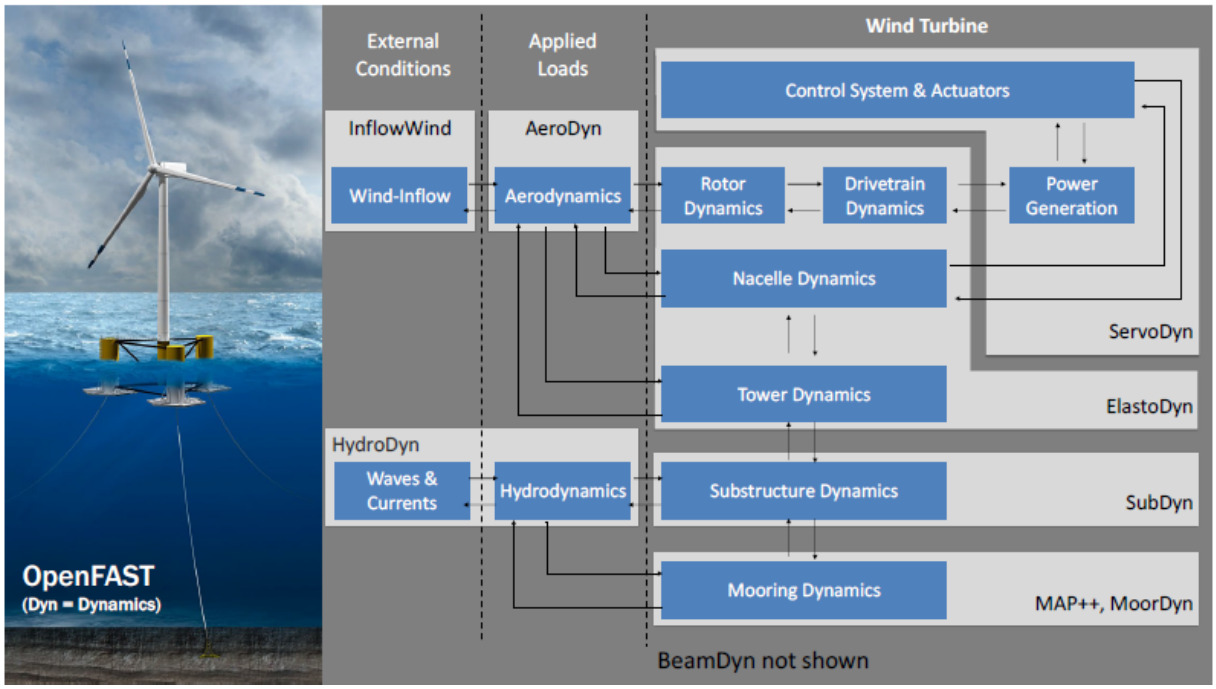

Figure 2.8: OpenFAST schematics. Figure from [16]

2.3.1. Modules

All of the modules are called by the main OpenFAST input file, formatted in ".fst" type, which contains the major simulations settings, the main environmental conditions, and the module files pathways.
In the following sections, a brief explanation of each module is given [4, 16].

AeroDyn

AeroDyn v15 is the time-domain aerodynamics module for horizontal-axis wind turbines. It calculates aerodynamic loads on both blades and tower, based on the principles of actuator lines. The influence of the wake is based on BEMT, integrated with corrections that can be optionally applied, while unsteady airfoil aerodynamics models include the ones described in Section 2.2.2. The loads calculations differ according to the selected options on AeroDyn: the wake model can be changed between BEMT and DBEMT through the *WakeMod* line, and the dynamic stall model thorugh *UAMod* and *AFAeroMod*.

BEMT	WakeMod=1, AFAeroMod=1
DBEMT	WakeMod=2, AFAeroMod=1
DBEMT & Dyn Stall	WakeMod=2, AFAeroMod=2
B-L 4-states model	UAMod=4
B-L 5-states model	UAMod=5
Øye model	UAMod=6

Table 2.1: Aerodynamics options in *Aerodyn*

AeroDyn is divided in submodules: rotor wake/induction, blade airfoil aerodynamics, tower influence, tower drag, aeroacustic, and buoyancy (for marine hydrokinetic turbines). The primary input file contains modeling options, environmental conditions, airfoils, tower characteristic and buoyancy properties. Airfoil data are defined from specific files and include aerodynamic coefficients and unsteady aerodynamics parameters. Blade characteristics are also described in a separated file. AeroDyn, in coupled mode, receives structural position, orientation and velocities as well as the undisturbed wind velocity.

ElastoDyn

ElastoDyn is the module responsible for the dynamics of the turbine structure, computing displacements, velocities, acclerations and reaction loads. It combines modal (blades, tower) and multi-body (platform, nacelle, generator, gears, hub tail) formulations, useful for different turbine configurations. The 3-bladed HAWT solutions can include up to 24 DoFs, including the six DoFs of the substructure/floating platform.
In the main input file, geometry, mass/inertia, stiffness and damping coefficients are defined, together with the initial/fixed displacements and velocities. Additional characteristics for the blades and tower are provided in separated files. From the other modules, ElastoDyn receives information about aerodynamic and hydrodynamic loads, the sub-

structure reactions and commands from the controller.

InflowWind

InflowWind is the module for the undisturbed wind inflow processing. It can model different wind situations: steady, uniform but time varying, full-field turbulence and user defined. At each time step, InflowWind calculates the wind velocities at the needed positions, undisturbed from interaction with the wind turbine and dependent only on the parameters given inside the module files.
The main input file contains the steady wind options, while the other wind types characteristics are contained in connected additional files.

ServoDyn

ServoDyn is the module dedicated to the control and electrical part. The available control methods are: blade pitch, generator torque, nacelle yaw, high-speed shaft brake, tip brakes and cables. Simple methods can be implemented directly in the module main input file by providing the necessary parameters, as well as the simulations of special events (e.g. turbine startup, shutdowns), while more complex solutions require externally compiled routines or interfacing with other tools such as Simulink.
Some example routines are available in the repositories, additionally to simple Simulink models.

ExtPtfm

The ExtPtfm (external platform) module uses superelement properties of the support structure defined in the input files, such as mass, stiffness, damping and the time series of excitation forces, to calculate the reaction of the structure at the interface with the tower base.
In his master thesis, Ortolani [20] describes a procedure for imposing the motion law to the turbine through this module. This method was applied similarly in this work, for the pitch motion and for the surge, with simple adaptations.
The procedure begins by defining the periodic sinusoidal motion law for the position (θ_p) and its derivatives, velocity ($\dot{\theta}_p$) and acceleration ($\ddot{\theta}_p$), as:

$$\theta_p(t) = \theta_0 + \Theta \, \sin(\Omega_p \, t + \phi) \tag{2.28}$$

$$\dot{\theta}_p(t) = \Theta \, \Omega_p \, \cos(\Omega_p \, t + \phi) \tag{2.29}$$

$$\ddot{\theta}_p(t) = -\, \Theta \, \Omega_p^2 \, \sin(\Omega_p \, t + \phi) \tag{2.30}$$

with θ_0 being the initial position, Θ the amplitude, Ω_p the angular frequency, and ϕ the phase. In the case of only pitch motion, the other DoFs are blocked in the ElastoDyn module, so the response of the platform can be built as:

$$\underline{x}_{Ptfm}(t) = \begin{bmatrix} 0 \\ 0 \\ 0 \\ 0 \\ \theta_p(t) \\ 0 \end{bmatrix} \qquad \underline{\dot{x}}_{Ptfm}(t) = \begin{bmatrix} 0 \\ 0 \\ 0 \\ 0 \\ \dot{\theta}_p(t) \\ 0 \end{bmatrix} \qquad \underline{\ddot{x}}_{Ptfm}(t) = \begin{bmatrix} 0 \\ 0 \\ 0 \\ 0 \\ \ddot{\theta}_p(t) \\ 0 \end{bmatrix} \tag{2.31}$$

In general, the equation of the response of the system, characterized by mass [M], damping [C] and stiffness [K] matrices, to a time-varying load $\underline{F}(t)$ is defined as:

$$[M]\,\underline{\ddot{x}}(t) + [C]\,\underline{\dot{x}}(t) + [K]\,\underline{x}(t) = \underline{F}(t) \tag{2.32}$$

In OpenFAST, the matrices combine both the platform and the turbine data (e.g. mass),

$$[M] = [M_{turb}] + [M_{Ptfm}] \tag{2.33}$$

while the load is made of the hydrodynamic forces from the waves/sea, which cause the platform motions, and the aerodynamic ones.

$$\underline{F}(t) = \underline{F}_{hyd}(t) + \underline{F}_{aero}(t) \tag{2.34}$$

In order to impose a prescribed oscillating motion, this procedure assigns very high values, many orders of magnitude higher than the turbine ones, to the platform characteristics, rendering the contribution of the rest of the machine negligible. The platform matrices, which can be written in a file read by the main ExtPtfm input file (from here on named "ExtPtfm_SE"), are made as follows (mass matrix in kg is reported as an example):

$$[M_{Ptfm}] = \begin{bmatrix} 0 & 0 & 0 & 0 & 0 & 0 \\ 0 & 0 & 0 & 0 & 0 & 0 \\ 0 & 0 & 0 & 0 & 0 & 0 \\ 0 & 0 & 0 & 0 & 0 & 0 \\ 0 & 0 & 0 & 0 & 1e30 & 0 \\ 0 & 0 & 0 & 0 & 0 & 0 \end{bmatrix} \tag{2.35}$$

Now, known the motion law and the above-mentioned values, the hydrodynamic force vector can be computed as:

$$[M_{Ptfm}]\,\underline{\ddot{x}}_{Ptfm(t)} + [C_{Ptfm}]\,\underline{\dot{x}}_{Ptfm(t)} + [K_{Ptfm}]\,\underline{x}_{Ptfm(t)} = \underline{F}_{hyd}(t) \tag{2.36}$$

$\underline{F}_{hyd}(t)$ can be calculated externally (for example through a Matlab script) for the whole simulation time and written as a time series composed of the time, null columns for the blocked DoFs, and the non-null one of interest, in the ExtPtfm_SE file.
In the end, when OpenFAST is run, the calculation of the whole system response will consider the forces in this module, which will overwhelm every other component characteristics, resulting in the system following the platform and its prescribed motion $\underline{x}(t) \approx \underline{x}_{Ptfm}(t)$.

Other modules

Below is a list of additional modules that are available in OpenFAST, however, they were not used in this work, so they are reported only for completeness:

- HydroDyn: hydrodynamics for fixed and floating substructures, waves;
- MoorDyn: mooring lines dynamics;
- SubDyn: alternative module for the substructure dynamics;
- BeamDyn: beam theory for the blade dynamics, to be coupled to ElastoDyn;
- IceDyn: module for ice loads.

3 | 5MW turbine

3.1. 5MW baseline turbine

The initial analysis of this thesis pertains to the simulation of the "NREL offshore 5MW baseline wind turbine" [17], a large machine that was created to be representative of both typical utility-scale land-based and offshore turbines. This realistic and standardized input data is available in the OpenFAST repository [1], which provides complete module input files. The fundamental properties of this turbine are outlined in Table 3.1.

Rating	5 MW
Rotor orientation, Configuration	Upwind, 3 blades
Rotor, Hub Diameter	126 m, 3 m
Hub Height	90 m
Cut-In, Rated, Cut-Out Wind Speed	3 m/s, 11.4 m/s, 25 m/s
Cut-In, Rated Rotor Speed	6.9 rpm, 12.1 rpm
Overhang, Shaft Tilt	5 m, 5°
Rotor Mass	110000 kg

Table 3.1: Main properties of the 5MW baseline turbine

3.2. OpenFAST files changes

The OpenFAST input files utilized in Zappulla's master thesis [26], were taken as a starting point for this study, as it begins by reproducing part of her work to identify potential model changes.

Primarily, it is essential to note that the proper functionality of the code is dependant on the lines of the files matching the order required by the selected version of OpenFAST. Consequently, the input files were adapted from version 3.1 to version 3.4.1 following the annotations reported in the "API changes between versions" section of the manual [3]. The majority of the changes concerned the buoyancy parameters specific to a marine

turbine, as well as the rotor and tail furling options in AeroDyn, although these alterations were not pertinent to the scope of this study. Nevertheless, an interesting update in the v3.4 fixed an issue within the Øye dynamic stall model, correcting the formulation of the separation function, which will be discussed next.
The analyses of the 5MW turbine focus on the aerodynamic loads that arise when the turbine operates close to its rated conditions ($\Omega = 12$ rpm, $U_0 = 11$ m/s) and is subjected to a sinusoidal pitch motion of the floating platform. These forces are implemented in the ExtPtfm_SE module.

3.3. Extreme pitching results

The case of "Extreme pitching motion", as documented by Zappulla [26], was replicated using the OpenFAST settings described in her work. Specifically, this simulation assumes more severe sea conditions, resulting in a sinusoidal pitch motion characterized by a frequency of 0.2 Hz and an amplitude of 4 deg. DBEMT simulations including dynamic stall models (*UAMod* equal to 4, 5 or 6) were taken into consideration.
The "new" outcomes for the "Extreme pitching motion" scenario, simulated in OpenFAST 3.4.1, are detailed in Tables 3.2 and 3.3. These tables present mean and peak values computed across the entire run time, enabling a comparison with the previously established "old" reference data.
While the B-L dynamic stall models remain practically unchanged from the preceding version of the code, a significant difference is evident in the Øye model.

POWER [MW]				
UAMod	**Old**		**New**	
	Mean	**Peak**	**Mean**	**Peak**
4	5.87	12.69	5.87	12.68
5	6.05	13.71	6.05	13.68
6	7.17	14.64	5.81	12.05

Table 3.2: Extreme pitching mean and peak power results

THRUST [KN]				
UAMod	Old		New	
	Mean	Peak	Mean	Peak
4	648.2	1100	648.1	1100
5	661.2	1167	661.2	1166
6	779.8	1255	641	1056

Table 3.3: Extreme pitching mean and peak thrust results

In the old charts depicted on the left side of Figure 3.1, where "UA" denotes *UAMod*, it is readily apparent that the UA6 trend is significantly detached from the rest, exhibiting values even greater than those of the computational fluid dynamics (CFD) results [26]. In contrast, in the new charts, the Øye model shows a similar albeit slightly lower behavior compared to the others, aligning more closely with the results obtained when switching-off dynamic stall models. This observation is more reasonable considering its simpler formulation as seen in Chapter 2.2.2. Furthermore, this model displays a minor phase shift when compared to the other two lines, and its trend is visibly smoother and more symmetrical. These attributes make it closer to the expected real-world response.

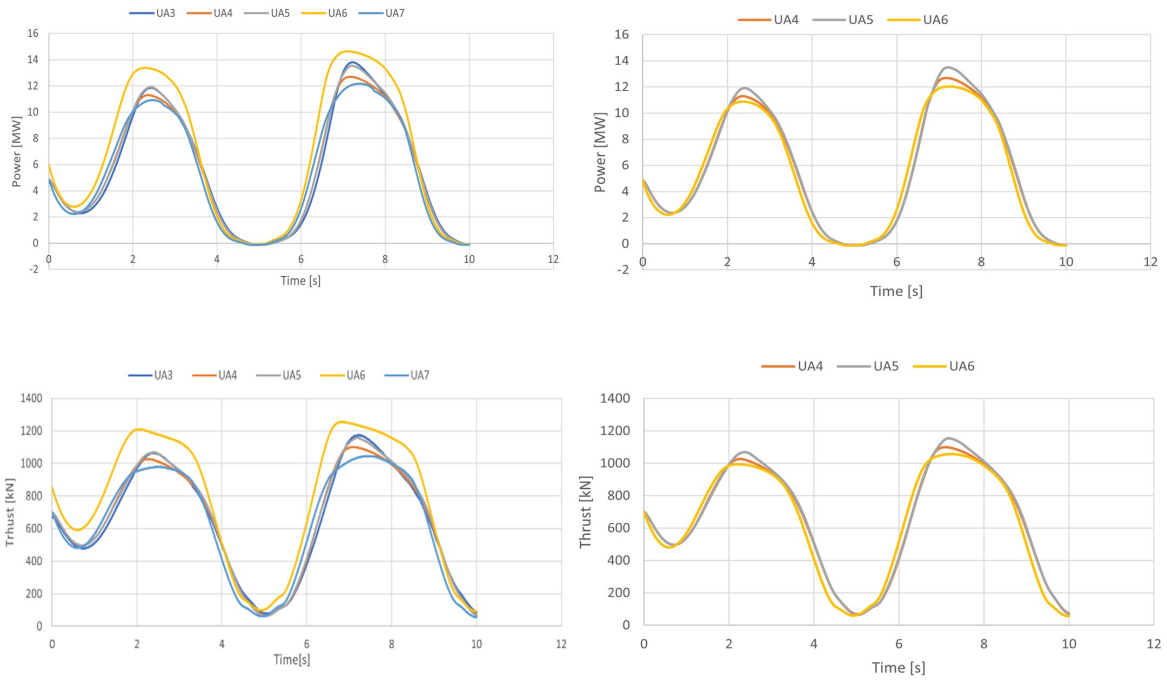

Figure 3.1: Comparison between old results [26] (left) and new ones (right)

3.4. 9 pitch cases

This second analysis centers on the reproduction of the pitch motion cases outlined in the study by Ortolani et al. [21], a reference also employed in the cited previous works [20, 26]. These simulations involve the application of pitch platform motions to the 5MW turbine, utilizing an OpenFAST setup akin to the previous one. The selected amplitudes are $\Theta = 1, 2, 4$ degrees, while the frequencies are set at $f = 100, 50, 25$ mHz, all featuring a phase shift of $\phi = 0$, between rotor revolution and platform motion. In total, this results in nine distinct cases.

3.4.1. Past data comparison

The initial set of results involves all the cases, comparing OpenFAST simulations with DBEMT and *UAMod* values of 4, 5, and 6 with the available data from the study [21], where an earlier version of OpenFAST was employed and coupled with the Minemma-Pierce formulation of the Beddoes-Leishman unsteady stall model ($UAMod = 3$).
Tables 3.4 and 3.5 report the percentage differences of the mean, maximum, and minimum power and thrust force values in comparison to the paper's results. Notably, the new simulations exhibit a high degree of similarity among themselves, while also being higher than the $UAMod = 3$ outputs. Furthermore, the most significant disparities generally emerge when the pitch motion amplitude is small, progressively reducing as Θ increases. Lastly, in the case where $f = 100$ mHz and $\Theta = 4$ deg, results are highlighted in blue as they show agreement between the models, particularly for the maximum values. A change of trend in two of them is exhibited: UA4 and UA6 show lower peaks than the reference one by -0.29% and -0.93%, respectively, for power, and -0.63% and -1.45% for thrust. Meanwhile, UA5 demonstrates a close, still slightly higher peak.

Table 3.4: 5MW nine cases power characteristics differences

POWER [%]										
		f100			**f50**			**f25**		
	UA	**Θ1**	**Θ2**	**Θ4**	**Θ1**	**Θ2**	**Θ4**	**Θ1**	**Θ2**	**Θ4**
mean	**4**	3.97	3.36	1.91	4.41	4.04	3.30	4.54	4.43	4.08
	5	3.91	3.35	2.17	4.34	3.98	3.26	4.47	4.35	4.01
	6	3.97	3.34	1.74	4.41	4.04	3.29	4.54	4.43	4.07

		f100			f50			f25		
	UA	**Θ1**	**Θ2**	**Θ4**	**Θ1**	**Θ2**	**Θ4**	**Θ1**	**Θ2**	**Θ4**
max	**4**	2.30	1.11	-0.29	3.43	2.45	1.22	4.13	3.47	2.50
	5	2.25	1.12	0.03	3.36	2.40	1.17	4.05	3.40	2.45
	6	2.38	1.13	-0.93	3.43	2.45	1.17	4.11	3.45	2.48
min	**4**	5.68	6.52	6.27	5.29	5.69	6.30	4.99	5.24	5.69
	5	5.62	6.52	6.65	5.22	5.64	6.30	4.92	5.16	5.60
	6	5.48	5.95	4.18	5.29	5.69	6.30	4.99	5.24	5.72

Table 3.5: 5MW nine cases thrust characteristics differences

THRUST [%]										
		f100			**f50**			**f25**		
	UA	**Θ1**	**Θ2**	**Θ4**	**Θ1**	**Θ2**	**Θ4**	**Θ1**	**Θ2**	**Θ4**
mean	**4**	3.80	3.45	2.27	4.00	3.82	3.42	4.04	4.00	3.84
	5	3.74	3.43	2.45	3.93	3.77	3.38	3.97	3.94	3.78
	6	3.78	3.39	2.04	3.99	3.82	3.40	4.04	4.00	3.83
max	**4**	2.78	1.81	-0.63	3.43	2.82	1.82	3.79	3.45	2.83
	5	2.74	1.81	0.32	3.38	2.78	1.77	3.71	3.39	2.79
	6	2.82	1.75	-1.45	3.43	2.82	1.77	3.79	3.43	2.82
min	**4**	4.63	4.84	3.86	4.44	4.67	4.81	4.29	4.44	4.67
	5	4.60	4.80	4.04	4.38	4.60	4.77	4.23	4.38	4.60
	6	4.53	4.50	2.41	4.44	4.66	4.77	4.29	4.44	4.67

The actual power and thrust values are provided in the following Tables 3.6 and 3.7. Additionally, they include the reference value from the paper as "ref", with the blue highlights indicating the same data points observed in the previous tables.

Table 3.6: 5MW nine cases power characteristics

POWER [MW]										
		f100			f50			f25		
	UA	Θ1	Θ2	Θ4	Θ1	Θ2	Θ4	Θ1	Θ2	Θ4
mean	ref	4.686	4.778	5.117	4.654	4.680	4.769	4.645	4.650	4.666
	4	4.872	4.939	5.215	4.859	4.868	4.926	4.856	4.856	4.857
	5	4.869	4.938	5.228	4.856	4.866	4.924	4.852	4.853	4.854
	6	4.872	4.938	5.206	4.859	4.868	4.926	4.856	4.856	4.856
max	ref	5.967	7.322	9.778	5.303	5.964	7.325	4.968	5.301	5.962
	4	6.104	7.403	9.750	5.485	6.110	7.414	5.173	5.485	6.111
	5	6.101	7.404	9.781	5.481	6.107	7.411	5.169	5.481	6.108
	6	6.109	7.405	9.687	5.485	6.110	7.411	5.172	5.484	6.110
min	ref	3.467	2.471	1.052	4.026	3.460	2.462	4.328	4.029	3.463
	4	3.664	2.632	1.118	4.239	3.657	2.617	4.544	4.240	3.660
	5	3.662	2.632	1.122	4.236	3.655	2.617	4.541	4.237	3.657
	6	3.657	2.618	1.096	4.239	3.657	2.617	4.544	4.240	3.661

Table 3.7: 5MW nine cases thrust characteristics

THRUST [kN]										
		f100			f50			f25		
	UA	Θ1	Θ2	Θ4	Θ1	Θ2	Θ4	Θ1	Θ2	Θ4
mean	ref	672.5	670.3	661.4	672.5	672.1	669.4	672.6	672.3	671.2
	4	698.0	693.4	676.4	699.4	697.8	692.4	699.7	699.2	697.0
	5	697.7	693.3	677.5	699.0	697.4	692.1	699.3	698.8	696.6
	6	697.9	693.0	674.9	699.4	697.7	692.2	699.7	699.2	697.0
max	ref	758.8	835.8	957.8	716.8	758.8	835.8	694.8	716.7	758.8
	4	779.9	850.9	951.8	741.4	780.2	851.0	721.1	741.4	780.3
	5	779.6	850.9	960.9	741.0	779.9	850.6	720.6	741.0	780.0
	6	780.2	850.4	943.9	741.4	780.2	850.6	721.1	741.3	780.2
min	ref	584.8	497.9	331.5	628.3	584.2	496.8	650.4	628.4	584.5
	4	611.9	522.0	344.3	656.2	611.5	520.7	678.3	656.3	611.8
	5	611.7	521.8	344.9	655.8	611.1	520.5	677.9	655.9	611.4
	6	611.3	520.3	339.5	656.2	611.4	520.5	678.3	656.3	611.8

In Figure 3.2, the thrust force is depicted (with the equivalent power graph, resembling

the thrust behavior, found in Appendix Figure A.1) for the nine cases, with the reference results from the paper labeled as "Ref". On the x-axis, t/T_{rev} is a dimensionless time variable used to plot the progression of the outputs throughout the pitching cycles. Here, t is the time and T_{rev} stands for the period of one rotor revolution, computed using 12 rpm or a rotor frequency of 200 mHz. In this figure, for the sake of visual clarity, Θ is denoted as "a", with the cases identified as "a" followed by the amplitude value, and "f" followed by the frequency. These two notations persist across all the figures of the analysis.

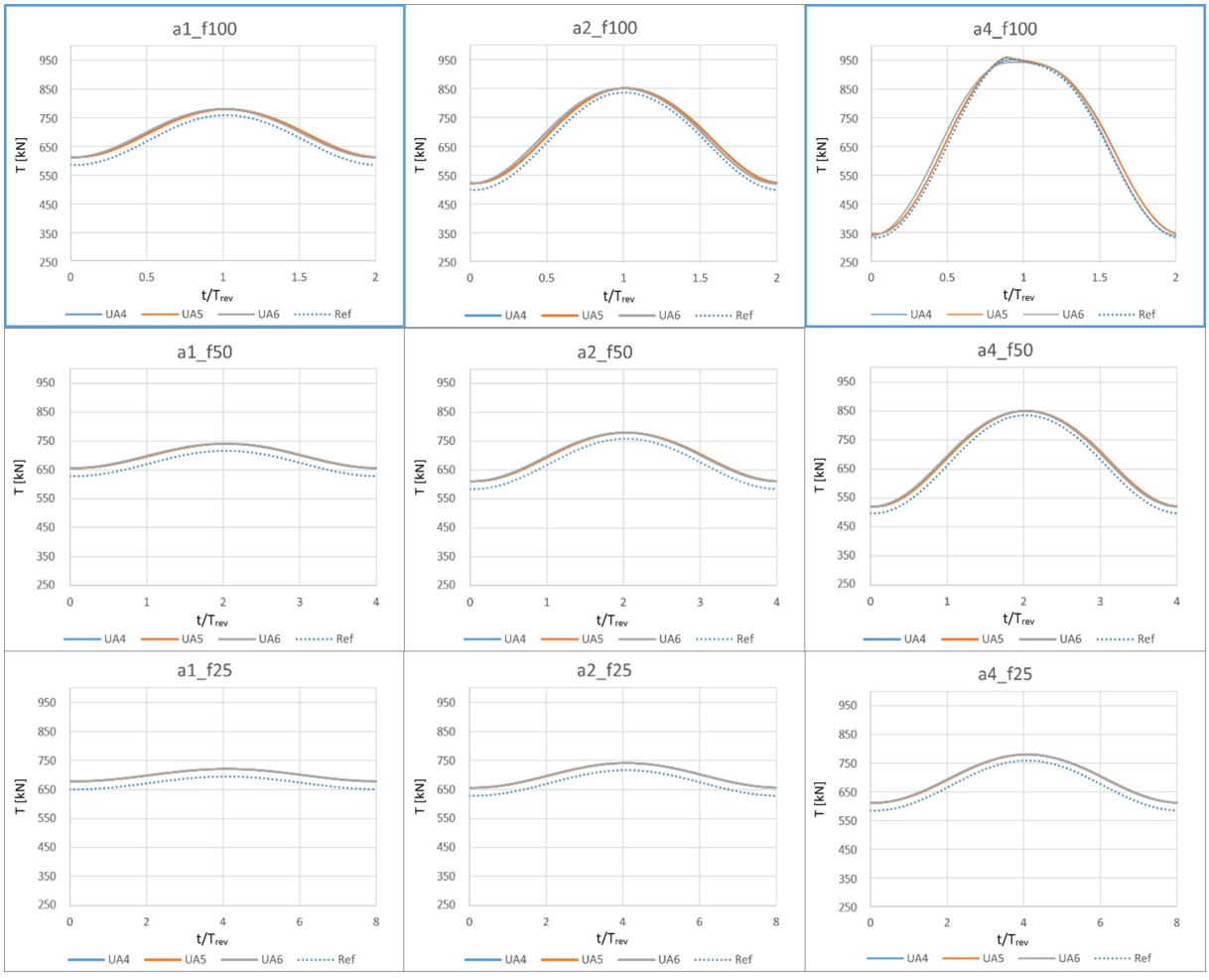

Figure 3.2: Thrust of the 5MW nine simulated cases

First, the main shape of the thrust output becomes apparent: the maximum corresponds to the windward movement of the turbine, where the rotor experiences an augmented wind speed compared to the undisturbed one. On the contrary, the minimum is present when the machine moves leeward, in the opposite direction. This general pattern applies to the power output as well.

Furthermore, the convergence of the results with the paper is more evident within these graphs. Once again, the "UA" cases closely align, while the "Ref" values diverge depending on the conditions. In these graphs, the impact of increased motion amplitude is visible moving to the right, though this effect is attenuated at lower frequencies. The most extreme instance is the before mentioned "a4_f100", which shows the least consistent behavior at its peak, leading to further examination in the next sections. Another of the eight remaining cases, specifically "a1_f100", was also subjected to additional analyses as a representative of the other similar, smoother cases.

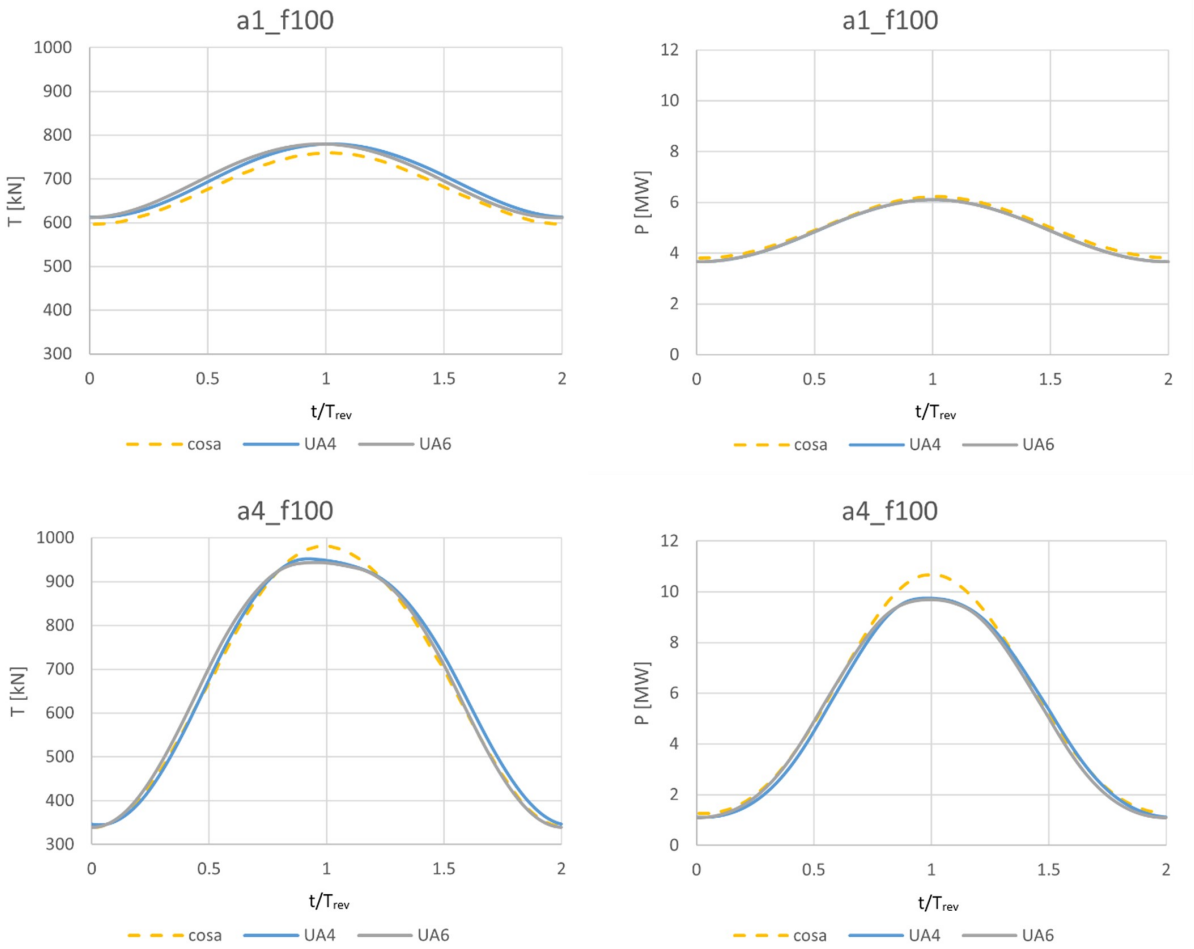

Figure 3.3: Comparison with COSA results

The last Figure 3.3 in this section shows a comparison with the CFD results from the COSA software, as depicted in the paper. As the data was not directly accessible, the trends were graphically extracted using a tool [2], introducing some expected imprecision. As mentioned before, only cases a1_f100 and a4_f100 are showcased. Furthermore, UA5

was excluded because it presented, at maximum, a convergence issue similar to the one investigated in past analyses [26], so the study continued with the more promising UA4 and UA6.
Across the DBEMT models, the thrust values generally surpassed those of the CFD, with this trend being more important in thrust than in power. This difference is due to the overall thrust being more influenced by the root region of the blade compared to the overall power, where, as it is further detailed in the next section, flow detachment is more evident but difficult to estimate both with CFD calculations as well as with BEMT.
Another notable feature in this figure is the difficulty of the DBEMT models in capturing the maximum values, especially accentuated in the higher amplitude case. Conversely, while there is a mismatch in minimum values, it is much smaller.

3.4.2. Dynamic models comparison

In order to have a complete overview of the dynamic effects, the analysis of the previously mentioned two cases is further extended by simulating the turbine with other options: deactivating all the dynamic models, so using steady BEMT (labeled as "BEM"), and with only the dynamic wake (labeled as "DBEM").
Figure 3.4 shows the thrust and power obtained from altering the dynamic models settings. To provide a comprehensive view, the y-axes are scaled accordingly, and two pitch periods are reported to visualize the lowest values. In the upper case, the results are fairly consistent except for the minimum values. In the power charts, this trend is confirmed, and variations are also noticeable in the maximum data points.

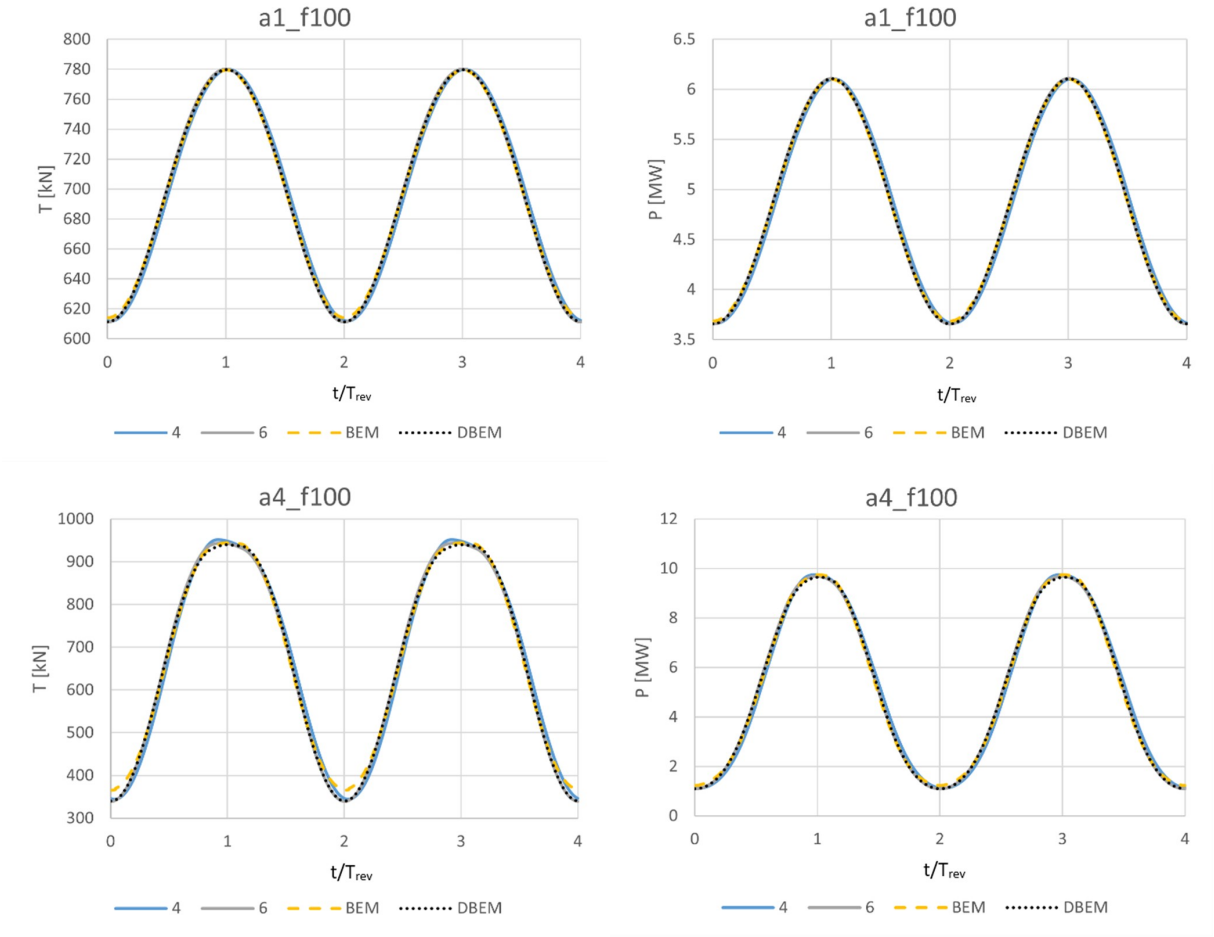

Figure 3.4: BEM, DBEM, and dynamic stall models comparison

Focusing on these crucial positions, Figure 3.5 highlights the distinctions in the thrust results: BEM has the smallest amplitude of values and presents the most symmetrical pattern. DBEM and UA6 output remarkably similar trends in the minimum section. However, while in the maximum DBEM seems to follow the steady formulation better, the Øye model simple formulation manages to capture the more relevant C_l dynamic variations at the peak. Moreover, UA4 demonstrates a delayed response united with an asymmetric peak, the highest among the results due to its more complex formulation.

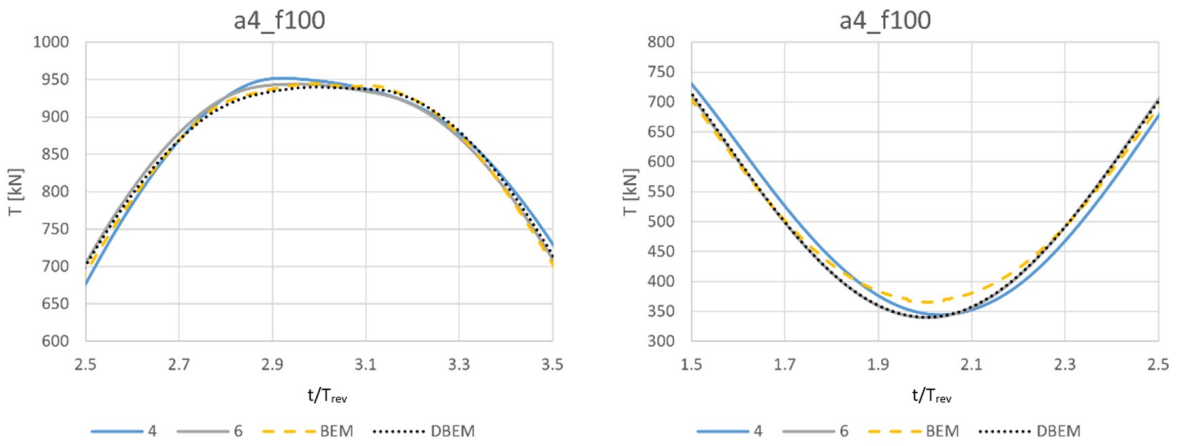

Figure 3.5: BEM, DBEM, and dynamic stall models comparison zoom-in

The previously described behavior can be attributed to certain blade parameters, in particular the AoA, followed by C_l and C_d. The following figures depict the local values along 18 nodes distributed along the blade. Additionally, the differences between the results, referred to the most complex UA4 simulations, are displayed in the bar plots.
At both the minimum and maximum points, the value of t/T_{rev} is an integer, indicating that the rotor has made a full rotation and the blades are positioned in their initial azimuthal configuration. The blade "1" assumes the vertical upward position, while, facing downwind, blade "2" and "3" are positioned as in Figure 3.6.

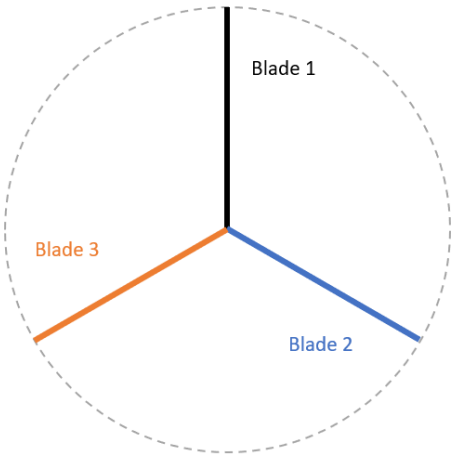

Figure 3.6: Azimuthal position of the blades

The first Figure 3.7 of this sequence shows the AoA of the minimum point, defined at t/T_{rev}=2. The trends are similar for all three blades so only blade 1 is reported here, while

the others are in Appendix A.2, A.3. The very low thrust and power values are mirrored by very low AoA: in some nodes of case a4_f100, α even exhibits negative values, due to the broader motion amplitude, which greatly impacts the felt wind speed and direction. The disagreement of the BEM model is visible in the lower graph, where it stands as the only one with discrepancies in α, especially towards the root. The other results are not visible in the figure as they are overlapped to the black line of DBEM.

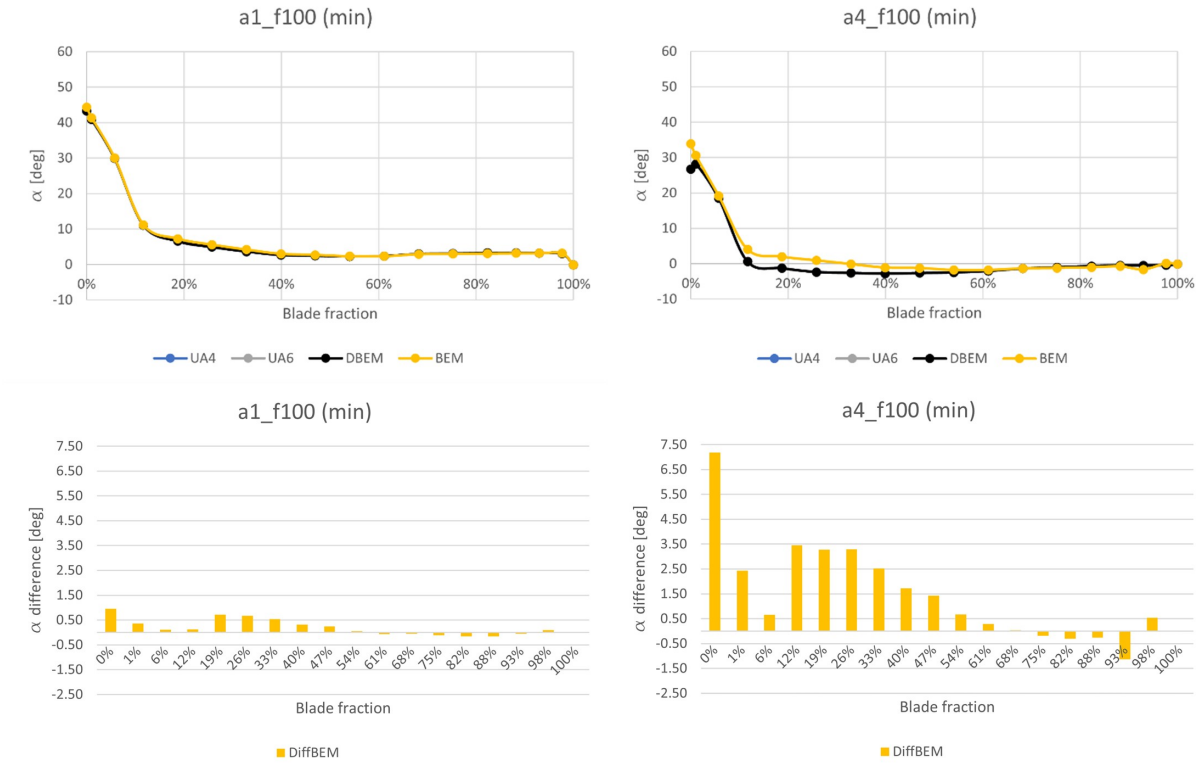

Figure 3.7: Minimum point AoA for the two cases

The next analysis is on the $t/T_{rev} = 3$ time step, around the maximum. This time the AoA of Figures 3.8 and 3.9 shows some difference between the blades due to their azimuthal position, however, they don't reveal significant variations between the models, so the focus moves to the aerodynamic coefficients.

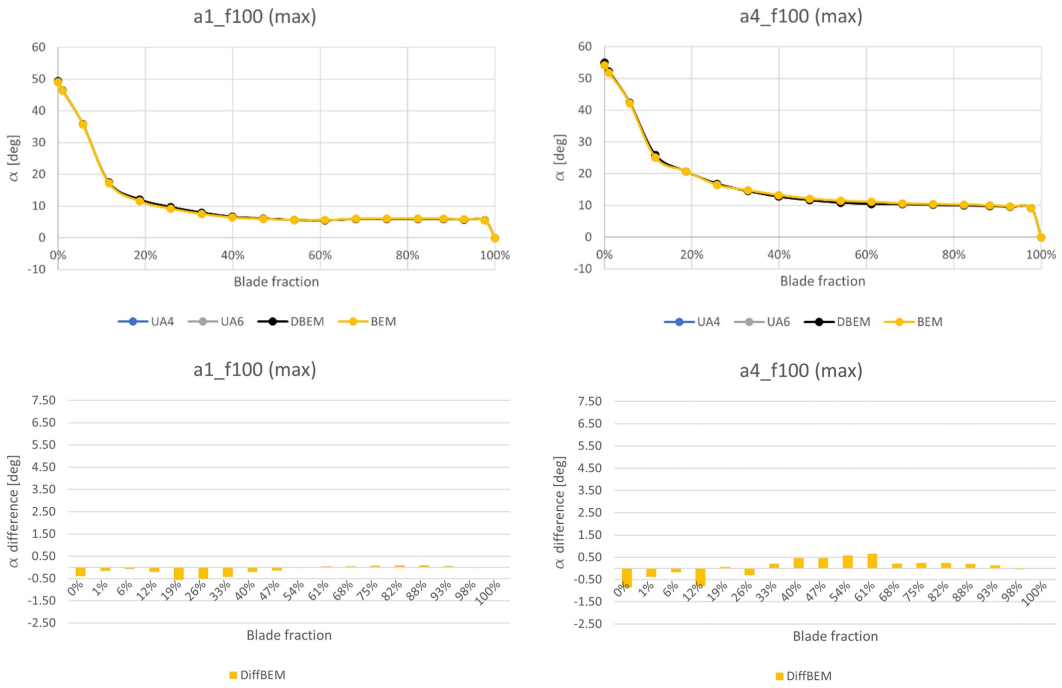

Figure 3.8: Maximum point AoA for the two cases. Blade 1

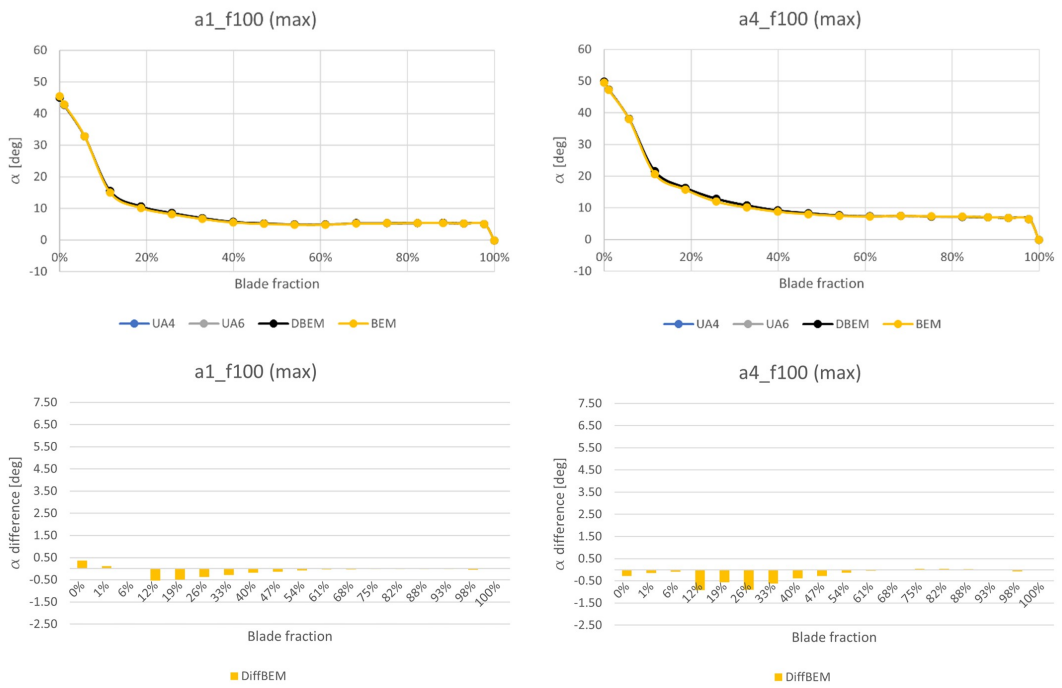

Figure 3.9: Maximum point AoA for the two cases. blade 2

The next graphs contain all three blades, as they display different trends.
The differences in C_l values in both $\Theta = 1$ and 4 deg are comparable, though more

pronounced in the latter case. Figure 3.11 shows the disagreement between the models in the first half of the blade, where BEM maintains the greatest separation from the reference UA4 (blue line). Among the blades, blade 2 displays the closest values to each other. This might be attributed to its slightly lower AoA compared to the other blades (as visible in Figure 3.9), leading to a more stable configuration. On the other hand, blade 3 has the largest differences, and it is interesting that towards the root, DBEM mostly aligns with BEM, suggesting that the effect of dynamic stall is possibly more relevant under those conditions.

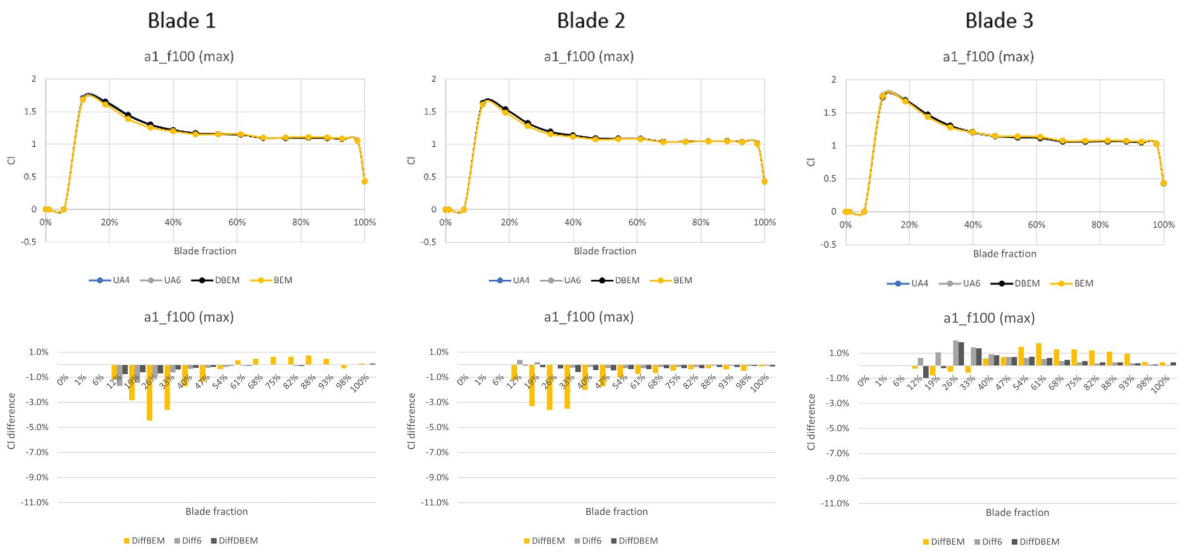

Figure 3.10: Maximum point C_l of the three blades for $\Theta = 1$ deg

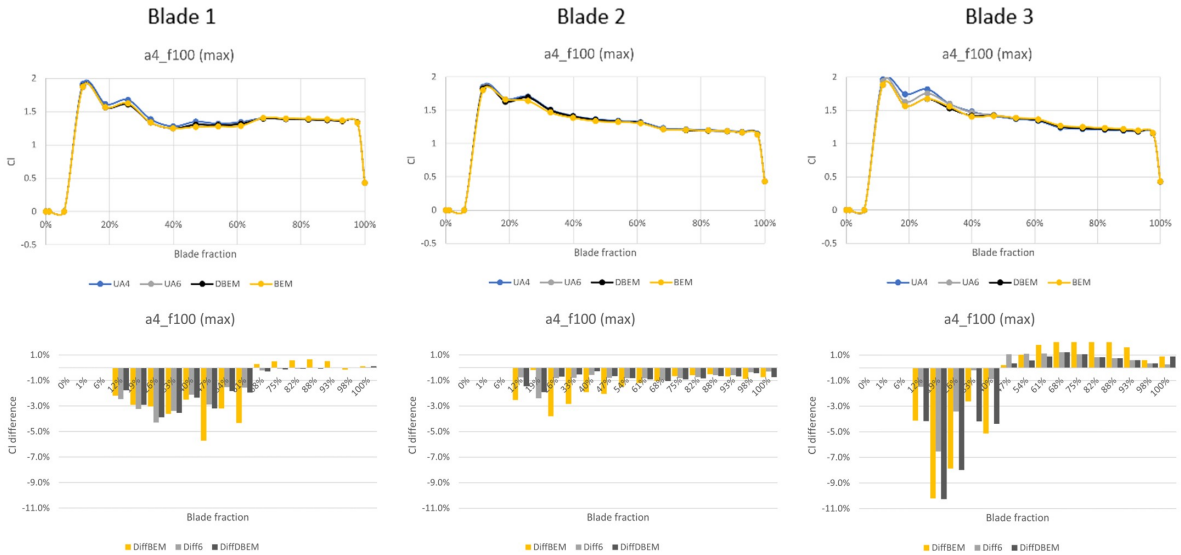

Figure 3.11: Maximum point C_l of the three blades for $\Theta = 4$ deg

Finally, the C_d exhibits analogous problems is the first half of the blades. The lower graphs of Figure 3.12 appear to indicate great percentage differences also toward the tip, but this is due to the absolute values being very close to zero.
Additional plots for the AoA the C_d are reported in the Appendix for completeness (A.4, A.5).

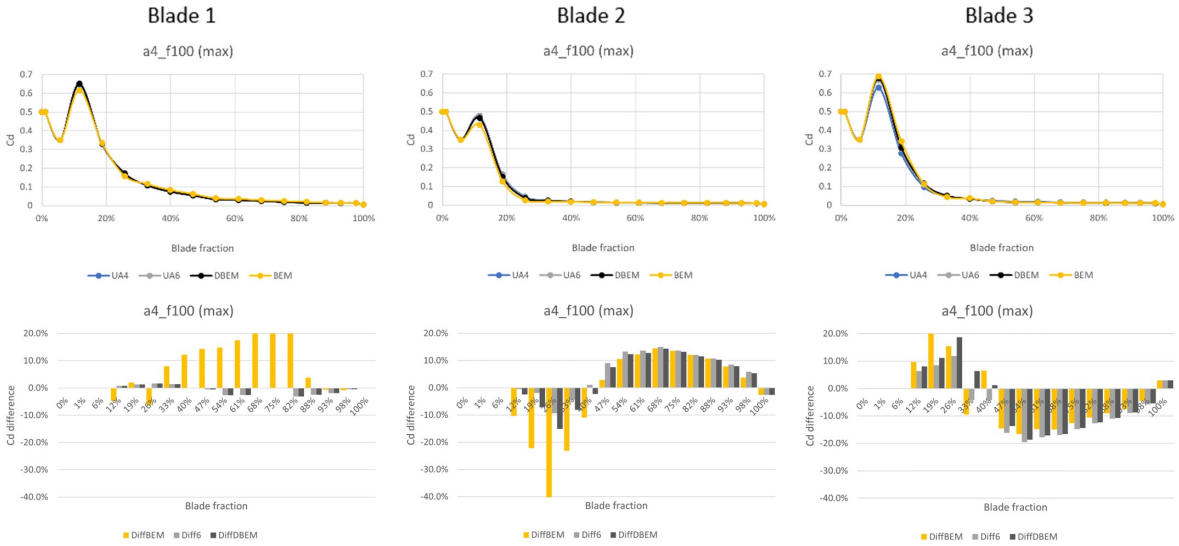

Figure 3.12: Maximum point C_d of the three blades for $\Theta = 4$ deg

4 | OC6 turbine

4.1. UNAFLOW project

The OC6 project [6, 22] bases its results on the experimental campaigns of the UNAFLOW project [5], which used a scaled turbine in the Politecnico di Milano wind tunnel.

4.1.1. Scaled turbine

The employed turbine is a 1:75 scaled model of the DTU 10MW Reference Wind Turbine. While utilizing the same rotor, different versions of the setup were used in the first (Ex1) or second campaign (Ex2), which correspond to surge-only, and additional surge and pitch tests, respectively. During Ex1, the turbine was mounted on hydraulic actuators, whereas in Ex2, it was affixed on a 6 DoFs robot. In both instances, load measurements were captured by a load cell situated at the top of the tower, complementing other forms of measurements.

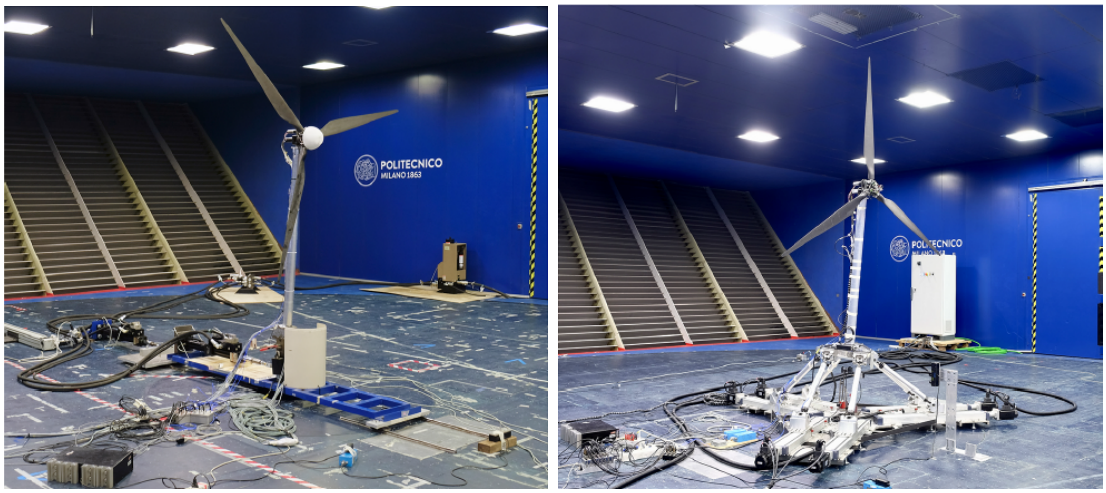

Figure 4.1: The scaled turbine configurations in the wind tunnel: (left) Ex1 and (right) Ex2. Figure from [6]

4.1.2. Geometry

The scaling approach was devised to preserve the thrust and power coefficients (C_t and C_p) of the full-scale machine. In order to minimize inertial disturbances, the tower was constructed as rigid, with the rotor tilted to counteract the pitch offset of the tower (5 deg) and to align it perpendicularly to the wind direction. Any remaining inertial components in the measurements were subsequently removed through filtering.
The geometry of the system is detailed in the table below, emphasizing the differences between the setups and the original full-size turbine.

Parameter	**Ex1**	**Ex2**	**DTU 10MW**
Rotor diameter	2.38132 m		178.3 m
Blade length	1.10166 m		86.37 m
Hub diameter	0.178 m		5.6 m
Tilt angle	5 deg		5 deg
Rotor overhang	0.09467 m	0.139 m	7.1 m
Tower-to-shaft distance	0.03667 m	0.064 m	2.75 m
Tower length	1.6057 m	1.4 m	115.63 m
Tower base offset	0.45 m	0.73 m	-

Table 4.1: Turbine geometry

The geometric parameters from the table are represented in the schematic of Figure 4.2.

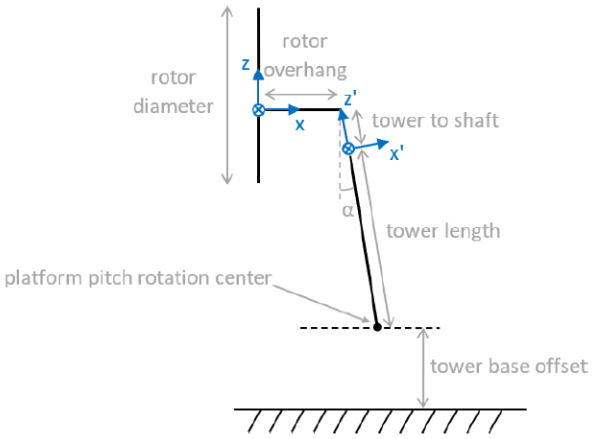

Figure 4.2: Turbine scheme and coordinate system. Figure from [6]

4.1.3. Blades

Due to the scaling, the wind velocity was scaled by a factor of 3 from the full-size conditions, and the resulting Reynolds numbers (Re) in the wind tunnel were reduced by a factor of 225. As a consequence, airfoils with low Re characteristics were chosen for the turbine blades. Specifically, the 10% thick version of the Selig Database SD7032 was employed. The blades were designed straight, with no coning angle, and were rigid, also the distributions of chord length and twist were adjusted to match the correct C_t and C_p. The aerodynamic coefficients C_l and C_d of the airfoil are provided at 20 radial stations and seven Re (5e4, 6e4, 7.5e4, 1e5, 1.5e5, 1.7e5 and 2e5). The two-dimensional aerodynamic polar data was initially obtained through testing, then, extrapolation to cover a AoA range of $-180/+180$ degrees was computed using the Viterna method. Furthermore, a transition section between circular section and airfoil profile was calculated by interpolation. Finally, three-dimensional stall delay corrections were applied to all the radial stations.

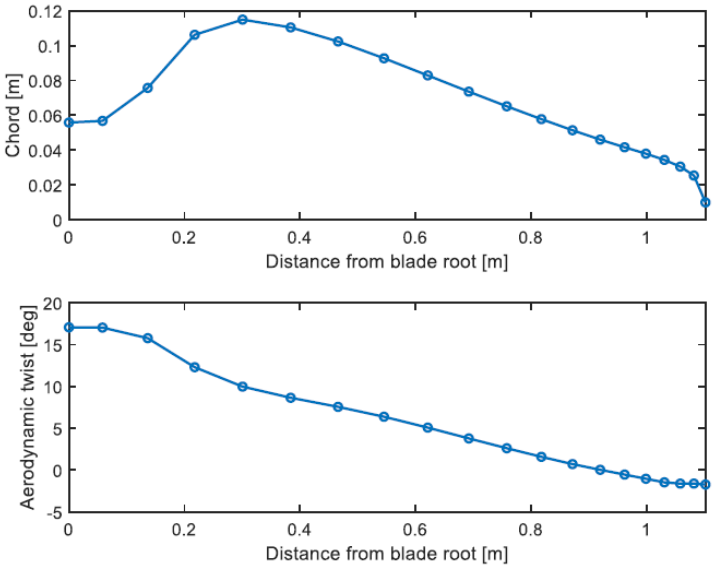

Figure 4.3: Chord and aerodynamic twist along the blade. Taken from [22]

4.1.4. Wind tunnel conditions

The experimental campaigns were conducted in the wind tunnel at Politecnico di Milano, with dimensions of 13.84 m in width, 3.84 m in height, and 35 m in length. The air density was considered at 1.177 kg/m^3. Achieving perfectly uniform wind flow was hindered by the influence of the tunnel walls and turbulence generated by the fans. The turbulence intensity was approximately 2%. The vertical wind profile, normalized by the wind speed

at the hub, and the turbulence are shown in Figure 4.4).
It is important to mention that the wind speed indicated for the simulations with the modeling tools is different from the actual one used in the wind tunnel. This difference is due to a correction made to account for blockage effects: the presence of the turbine in the test section leads to a reduction in the flow area compared to an unrestricted freestream, which results in increased wind velocity at the rotor disk. The wind speed was accordingly increased, for example, from 4 m/s to 4.19 m/s.

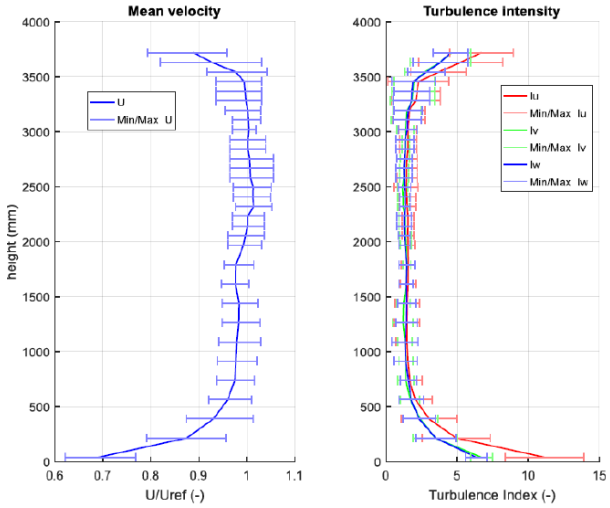

Figure 4.4: Wind tunnel flow characteristics. Taken from [22]

4.1.5. Load cases

The load cases contain two steady wind conditions along with the unsteady ones. The pitch motions were made in such a way that the horizontal apparent wind component at the rotor corresponded to the one in the surge motions (for instance, case 3.5 corresponds to case 2.5). The additional cases 2.12 and 2.17 lack experimental data, as they were used as verification for the impact of more significant flow conditions. The cases from the experimental campaigns that have been selected and replicated in this thesis are shown in Table 4.2.

Wind state	Load case	U_0 [m/s]	Platform motion			Rotor speed (Ω) [rpm]	Blade pitch angle [deg]
			Direction	f [Hz]	Amplitude [m] or [deg]		
Steady wind	1.1	4.19	none			240	0
	1.2	6.03				265	12.5
Unsteady wind	2.5	4.19	Surge	1	0.035	240	0
	2.12			2	0.08		1.5±1.5
	2.17						
	3.5		Pitch	1	1.4		0

Table 4.2: Replicated load cases

4.2. OpenFAST implementation

This section provides a detailed description of the changes made to the files. The starting point was the set of files of the 5MW Baseline turbine used in Section 3.3.
Given the incomplete nature of the OpenFAST manual [16], part of the information needed for generating the input files was also sourced from other documents including the "FAST v6 User's Guide" [18], the "FAST v8 README" [15], and additional manuals specific to individual modules.
All files requiring modifications were created through a dedicated Matlab script. The script printed every line with the necessary values and saved the files in their appropriate directory to respect the paths specified within the files themselves. Since a multitude of input files necessitated distinct values for each simulation, the Matlab scripts were designed to extract relevant data from external Excel tables. Subsequently, a new folder was generated containing the input files for each OpenFAST run.
The selection of outputs for each file was based on the available ones listed in the "OutListParameters" Excel file, as found in the manual. Then, to facilitate further use, the "ReadFASTtext" Matlab function from the OpenFAST repository [1], specifically from the matlab-toolbox, was used to create Matlab data results files.

4.2.1. Main

The main .fst file (which will be called "Main.fst") starts with a section dedicated to "simulation control". Due to the very fast rotational speed of the rotor and platform motion, $TMax$ was set to 20 seconds, simultaneously, DT was configured at 0.001 seconds,

adhering to the recommended rule of thumb of having at least 200 azimuth steps within a single rotor revolution.
In the "feature switches and flags" part of the file, the various modules can be activated. Across all the simulations, *CompElast* and *CompInflow* were set to 1, while *CompAero* was set to 2. Furthermore, *CompServo* was switched to 1 solely for case 2.16, while *CompSub* was set to 2 for all the cases involving unsteady conditions. The remaining switches were left to 0.
Concerning the "environmental conditions", *Airdens* was set to 1.177 kg/m^3, equal to the air density within the wind tunnel. Additionally, *SpdSound* and *Patm* were reset to the default values suggested by the OpenFAST manual, 340.3 m/s and 101325 Pa respectively.
Last, the "Input Files" section required the paths to the pertinent input files of the selected modules. In these simulations, the necessary ones were: *EDFile, InflowFile, AeroFIle, ServoFile* and *SubFile*. The remaining lines were marked with the entry "unused".
The rest of the main file was left unchanged.

4.2.2. AeroDyn

The AeroDyn module is set up by multiple files. The main input file (AeroDyn.dat) commences with the "General Options" section: *WakeMod* and *AFAeroMod* change according to Table 2.1, while the rest was left deactivated.
The *AirDens* line within "Environmental Conditions" was once again set to 1.177, while the "Blade-Element/Momentum Theory options" were all left activated, consistent with the referenced files, to encompass all necessary corrections to BEMT.
In the "Dynamic Blade-Element/Momentum Theory Options", *DBEMT_Mod* was left to 2 (time-dependent τ_1). Again, in the "Beddoes-Leishman Unsteady Airfoil Aerodynamics Options", the *UAMod* line follows the settings of Table 2.1, while *UAStartRAd* remained to its default value of 0, and *UAEndRad* of 1.
The "Airfoil Information" section calls the airfoil input files (Airfoil_i.dat) that were configured as explained in the next Section 4.2.3. *AFTabMod* was set to 2, reflecting the need for interpolation of the aerodynamic coefficients based on both AoA and Re. *InCol_Cm* was changed to 0 due to the absence of available data. Given that all of the available airfoil data were used, *NumAFfiles* was set to 20 and, consequently, *AFNames* includes 20 path lines corresponding to the airfoils files.
The next part "Rotor/Blade Properties", similarly needs the paths of the files related to the blades described in Section 4.2.4. Since the blades are identical, the three *ADBlFile* entries reference the same blade file.
The following three sections were ignored, while the "Tower Influence and Aerodynamics"

was configured, albeit the simulations not accounting for tower disturbances. Minimal information about the tower is required by OpenFAST to couple AeroDyn with ElastoDyn, so *NumTwrNds* was set to 10, and the properties table was filled as follows:

Table 4.3: Aerodyn tower characteristics

TwrElev [m]	TwrDiam [m]	TwrCd	TwrTI	TwrCb
0.0000000E+00	0.0750000E+00	1.0E+00	1.0E-01	0.0
1.7841111E-01	0.0750000E+00	1.0E+00	1.0E-01	0.0
3.5682222E-01	0.0750000E+00	1.0E+00	1.0E-01	0.0
5.3523333E-01	0.0750000E+00	1.0E+00	1.0E-01	0.0
7.1364444E-01	0.0750000E+00	1.0E+00	1.0E-01	0.0
8.9205556E-01	0.0750000E+00	1.0E+00	1.0E-01	0.0
1.0704667E+00	0.0750000E+00	1.0E+00	1.0E-01	0.0
1.2488778E+00	0.0750000E+00	1.0E+00	1.0E-01	0.0
1.4272889E+00	0.0750000E+00	1.0E+00	1.0E-01	0.0
1.6057000E+00	0.0750000E+00	1.0E+00	1.0E-01	0.0

where the first column comprises the equidistant tower elevation positions, from base to top, the second the constant tower diameter, the third the circular section C_d values, and the final two columns are reported with default values that remained unused.

4.2.3. Airfoils

Each Airfoil_i.dat file (the index "i" takes on values from 1 to 20 in the actual filenames) contains seven tables for each Re provided in the original files mentioned in Section 4.1.3. At the beginning of each file, *NumCoords* was set to 0 and *NumTabs* to 7 for the reason above.

After the "!data for table j" line (where index "j" goes form 1 to 7), the value of *Re* changes for each table, as well as the UA (Unsteady Aerodynamics) data. Among these coefficients, the majority were left at default values, with *alphaUpper* and *alphaLower* omitted as they can be calculated by the tool. The coefficients that were evaluated for every table were: *alpha0*, *alpha1*, *alpha2*, *C_n1*, *C_n2*, and *Cd0* (*Cm0* was set to 0, given the absence of C_m data). These numerical values were obtained using the "AeroDyn_UA_coefficients" Matlab function provided by Roger Bergua in the OpenFAST forum [19].

Finally, the table with the aerodynamic coefficients begins with an indication of the total line count, *NumAlf*, then, three columns were printed with, in order, the α, C_l, and C_d extracted from the provided files. Each Airfoil_i.dat file repeats after the line "! data for

table j" seven times to include every Re value.
As a last note, these files remained the same for every simulation.

4.2.4. Blade

A blade file (AeroDyn_blade.dat) is needed to incorporate the geometry of the blade and to match the airfoil to the correct radial position. This file is made of a table, populated with data sourced from the blade characteristics reported in [22]. A part of the table is shown below, with the 0-value columns omitted for better visualization.

Table 4.4: Aerodyn blade characteristics

BlSpn [m]	BlTwist [deg]	BlChord [m]	BlAFID
0.0000	17.0767	0.0558	1
0.0582	17.0420	0.0568	2
0.1364	15.7759	0.0757	3
0.2177	12.3051	0.1062	4
0.3006	9.9830	0.1149	5
0.3838	8.6514	0.1104	6
0.4658	7.5652	0.1024	7
0.5453	6.3816	0.0927	8
0.6210	5.0801	0.0829	9
0.6921	3.7904	0.0736	10
0.7578	2.6168	0.0652	11
0.8176	1.5909	0.0578	12
0.8715	0.7175	0.0514	13
0.9195	0.0375	0.0460	14
0.9617	-0.5351	0.0416	15
0.9986	-1.0339	0.0380	16
1.0306	-1.4625	0.0344	17
1.0581	-1.6117	0.0305	18
1.0816	-1.6071	0.0254	19
1.1017	-1.7224	0.0100	20

In this table, the first column corresponds to the radial positions, the second is the blade twist, the third is the chord length, and the last column refers to the "airfoil ID", which is the position of the file in the path list written within AeroDyn.dat under the *AFNames* line.

Lastly, analogous to the previous section, it is unnecessary to recreate this file for each simulation.

4.2.5. ElastoDyn

The ElastoDyn module also includes multiple files. The main file ElastoDyn.dat begins with the settings for the "Degrees of Freedom". Here, everything is set to False, with the exception of *PtfmSgDOF* or *PtfmPDOF*, which are switched to True in the cases involving surge or pitch, respectively.
In the "Initial conditions" part, the fixed parameters are: *RotSpeed* at 240 rpm, and *PtfmPitch* at -5 deg. The negative sign comes from the reference coordinates illustrated in Figure 2.2. For the three blades, the *BlPitch* entries are the same and are 0 for all the cases except for 1.2, where they are adjusted to 12.5 deg, and 2.17, where they are set to the initial 1.5 deg. The other values in this section were set to 0.
The next section, "Turbine Configuration", describes the geometry of the turbine. The inserted values come from Table 4.1 and information found in the OC6 documents [6, 22]. These numbers are reported below in Table 4.5. The geometry from Ex1 was used for the surge cases, while that from Ex2 was utilized for the pitch scenario. The unknown parameters were left at 0.

Surge	**Pitch**	**Parameter**
3		NumBl
1.1907		TipRad
0.089		HubRad
-0.09467	-0.139	OverHang
-5		ShftTilt
0.03667	0.064	Twr2Shft
1.6057	1.4	TowerHt

Table 4.5: ElastoDyn turbine configuration

The remaining sections within the file were left unaltered, as this data is not used in the simulations, due to the deactivation of the respective DoFs at the beginning. However, because of the coupling with AeroDyn, in the "Blade" section, *BldNodes* was set to 20 and *BldFile* was configured. Similarly, in the "Tower" part, the *TwrFile* was provided.

4.2.6. ElastoDyn blade and tower

As mentioned before, ElastoDyn.dat requires both a blade and a tower file. The tower file was left unchanged from the 5MW files and was simply linked to the main input, while modifications were required for the blade file, as detailed below.
Starting with the initial sections, *NBlInpSt* was changed to 20 and *AdjBlMs* to match the value for AD15. The data in the "Blade mode shapes" part was ignored, while the "Distributed blade properties" table was adapted to mirror the one of AeroDyn_Blade.dat. The first three columns were aligned with the referenced table, while the other three kept the values of the 5MW turbine, as they were unused. The specific numbers are reported below.

Table 4.6: ElastoDyn blade characteristics

BlFract	**PitchAxis**	**StrcTwst [deg]**	**BMassDen**	**Flpstff**	**EdgStff**
0.0000	0.0	17.0767	6.79E+02	1.81E+10	1.81E+10
0.0528	0.0	17.0420	7.33E+02	1.51E+10	1.96E+10
0.1238	0.0	15.7759	3.93E+02	5.30E+09	7.57E+09
0.1976	0.0	12.3051	4.07E+02	3.41E+09	7.09E+09
0.2729	0.0	9.9830	3.44E+02	2.21E+09	4.72E+09
0.3484	0.0	8.6514	3.25E+02	1.68E+09	4.09E+09
0.4228	0.0	7.5652	2.97E+02	1.13E+09	3.48E+09
0.4950	0.0	6.3816	2.62E+02	6.64E+08	2.71E+09
0.5637	0.0	5.0801	2.37E+02	3.87E+08	2.22E+09
0.6282	0.0	3.7904	1.96E+02	2.25E+08	1.53E+09
0.6879	0.0	2.6168	1.65E+02	1.25E+08	1.18E+09
0.7422	0.0	1.5909	1.43E+02	9.54E+07	8.59E+08
0.7911	0.0	0.7175	1.25E+02	7.29E+07	6.66E+08
0.8346	0.0	0.0375	1.02E+02	5.45E+07	4.82E+08
0.8730	0.0	-0.5351	9.24E+01	4.20E+07	4.10E+08
0.9065	0.0	-1.0339	7.75E+01	3.23E+07	3.27E+08
0.9355	0.0	-1.4625	6.71E+01	2.47E+07	2.68E+08
0.9604	0.0	-1.6117	5.34E+01	1.37E+07	1.24E+08
0.9818	0.0	-1.6071	4.43E+01	6.48E+06	7.75E+07
1.0000	0.0	-1.7224	1.03E+01	1.70E+05	5.01E+06

4.2.7. InflowWind

In this module, a completely uniform, constant-in-time type of wind was defined. The lines regarding coordinates and positions are not important, while *WindType* was set to 2, and the *Filename_uni* path was configured to the uniform wind file discussed in the next section.

4.2.8. Uniform wind

The uniform wind file contains a table of the attributes of the wind flow. Across all the cases, a horizontal, perfectly uniform, and constant wind of 4.19 (or 6.03) m/s was characterized using the first two columns, while the rest were put to 0.

Time [s]	Wind Speed [m/s]
0.0	4.19
0.1	4.19
999.9	4.19

Table 4.7: Uniform wind table

4.2.9. ExtPtfm

The base input file for the SubDyn module is the ExtPtfm.dat file, which was left unchanged with respect to the reference file, except for the *Red_FileName* line that contains the path to the ExtPtfm_SE.dat file explained in the following section.

4.2.10. ExtPtfm_SE

The theory behind the ExtPtfm_SE.dat file has been previously described in Chapter 2, Section 2.3.1. Nonetheless, the necessary modifications to the input are delineated here, alongside the few differences present between the cases.
First of all, for all cases, the top lines for "Time increment in simulation" and "Total simulation time in file" were changed to match the simulation control values in Main.dat, so 0.001 and 20 respectively. Then, the mass, stiffness, and damping matrices were written akin to the one shown in Matrix (2.35), however, the 1e30 value was inserted at that specific location only for the pitch case, while it must be placed in the first diagonal position for the surge DoF cases. Similarly, in the subsequent "Loading and wave elevation" section, the time column containing all the time steps is followed by the six of the forces: all values must be 0 except for the first column in surge cases, or the fifth one for the

pitch. The last column pertaining to wave elevation was also left empty.
The computations for loading within this segment were performed using an external Matlab file, starting from the motion Equations (2.28). Considering the reference coordinates and experiments [22], the phase ϕ is set to 180 deg for the surge cases and 0 for the pitch. Additionally, the pitch also has an initial position of -5 deg.
An example of the first few lines from the loading section is reported in the table below.

1 time column	**n force columns**					
0.000000e+00	-1.005310e+30	0.0	0.0	0.0	0.0	0.0
1.000000e-03	-8.474876e+29	0.0	0.0	0.0	0.0	0.0
2.000000e-03	-6.895317e+29	0.0	0.0	0.0	0.0	0.0
3.000000e-03	-5.314670e+29	0.0	0.0	0.0	0.0	0.0
...						

Table 4.8: ExtPtfm_SE file time-loading lines of a surge case

4.2.11. ServoDyn

This module was used only for case 2.17, aimed at implementing blade pitch control. Notably, this file had not been utilized in the previous work [26], so the most recent available version of the ServoDyn.dat file of the 5MW turbine was downloaded from the OpenFAST files.
The sole section of interest within it is the "Pitch control". Here, *PCMode* was set to 4 to enable the use of Simulink, with *TPCOn* equal to 0, and the remaining lines for override options were configured as follows: *TPitManS* to 9999.9, *PitManRat* to 8, and *BlPitchF* to 0.

4.2.12. Simulink model

The Simulink model employed in the simulations was based on the "OpenLoop.MDL" provided within the tool files. Because of the function it is based on, this model was accessed and edited using the 2020 version of Matlab.

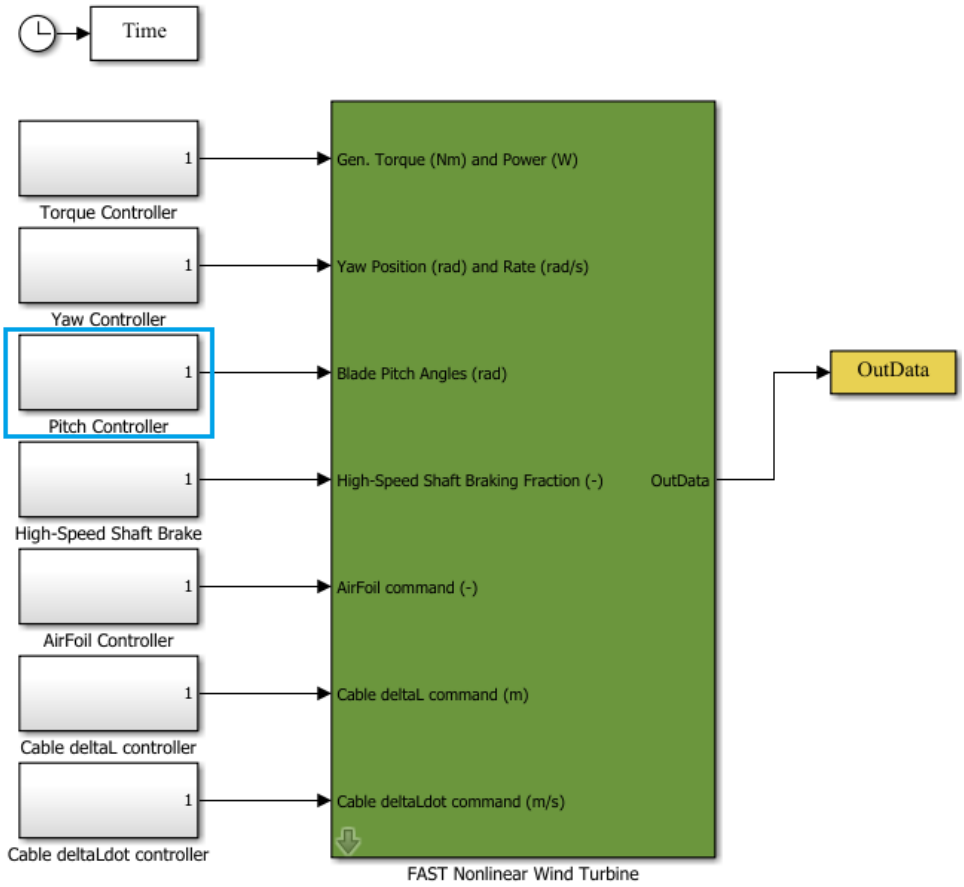

Figure 4.5: OpenLoop Simulink model

The OpenLoop model allows the actuation of several control strategies by imposing the wanted values in input. The component of interest within the model is the "Pitch Controller" block, highlighted in blue in Figure 4.5. Inside this element, in the baseline model, there is a constant block, which, for case 2.17, was modified to a "From file" block as shown in Figure 4.6.

Figure 4.6: Pitch controller block in the modified OpenLoop model

This change allows to input a Matlab data file (PitchInput.mat) containing the periodic pitch actuation profile showcased in Figure 4.7. The file is a matrix with four rows: the first is the time, while the other three are identical and indicate the pitch for each blade. The beginning segment of the matrix is reported as an example in Table 4.9.

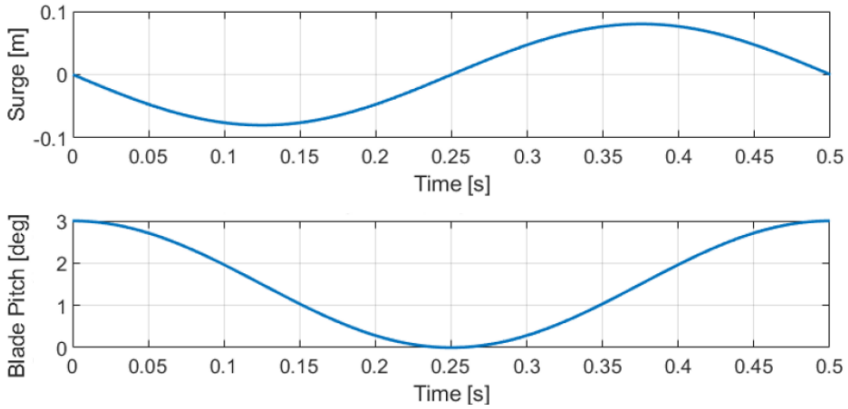

Figure 4.7: Periodic platform motion and blade pitch. Figure from [22]

Then, following the instructions in the old manuals [15, 18], OpenFAST can be executed through this Simulink model using a Matlab script (with the 2020 version) similar to the one used for the other cases, accessing files originally present in the OpenFAST binaries folder. As a final note, the outputs are directly converted into Matlab data format by the model.

0.0	0.001	0.002	0.003	
0.05234	0.0524	0.0524	0.0523	...
0.05234	0.0524	0.0524	0.0523	
0.05234	0.0524	0.0524	0.0523	

Table 4.9: First columns of the PitchInput.mat file

4.3. Results

The results obtained from the OpenFAST simulations mainly focus on power, thrust, and torque (Q). The torque is derived from the aerodynamic power using the formula:

$$Q = P/\Omega_p \tag{4.1}$$

where Ω_p, for the turbine rotating at 240 rpm, is equal to 25.13 rad/s (and at 265 rpm, it is 27.75 rad/s).
These specific outputs were selected because they can be compared with the results provided in the OC6 document [6]. This comparative analysis serves to verify the meaningfulness and validity of the simulations.

4.3.1. Steady wind

The first simulations concern the steady cases 1.1 and 1.2, which correspond to a rated and an above-rated condition, respectively. These cases were run with steady BEMT options in AeroDyn.dat.
The outputs are constant and yield the values in the following Table 4.10.

case	Thrust [N]	Torque [Nm]	Power [W]
1.1	34.93	3.01	75.62
1.2	16.31	2.11	58.59

Table 4.10: Steady wind cases results

For case 1.1, Figure 4.8 illustrates that the Ex1 produced $T = 36$ N and $Q \approx 3.25$ Nm, which are higher than the simulated numbers. Nevertheless, these BEMT results align with the median outcome achieved through the same approach by the participants to the OC6 project. As such, the differences of $T = 1.07$ N and $Q \approx 1.14$ Nm remain satisfactory. The utilization of the median instead of the mean in the figure is to mitigate the potential influence of outliers [6].
On the contrary, the results from case 1.2 seem to underestimate the power, as an above-rated configuration should not operate at such low production, while a -22.5% reduction can be observed from 1.1 to 1.2.

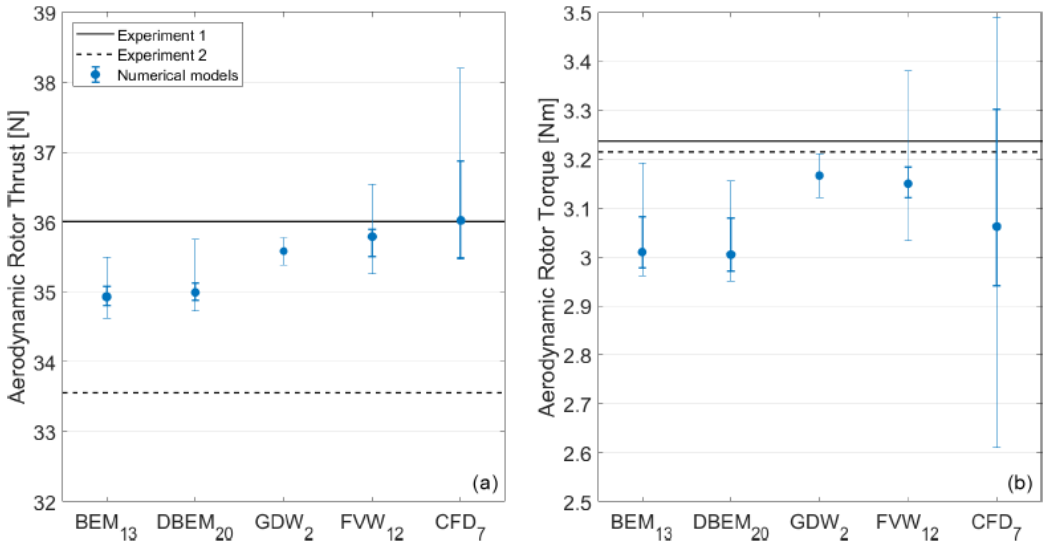

Figure 4.8: Aerodynamic rotor thrust (a) and torque (b) during the steady wind condition (case 1.1). Median and quartiles for the different simulation approaches. Figure from [6]

4.3.2. Unsteady wind

The following pages delve into the analysis of the unsteady wind cases, which are characterized as described in Table 4.2. Analogous to the 5MW turbine cases, the power/torque and thrust outputs exhibit a maximum when the machine is moving windward and a minimum when moving leeward, in the opposite direction. The graphs for pitch and surge cases are shifted by 180 degrees in phase, resulting in visual disparities, yet they retain the same main characteristics as mentioned earlier. On the x-axis, the "motion phase" is reported in degrees: a platform motion cycle starts at 0 deg to be completed at 360 deg. Two periods, extending to 720 deg, are reported to be able to observe the extremes. It is important to remember that the frequencies differ between cases, so a 360 deg period is completed in different amounts of time. Figure 4.9 shows an example of an output over the entire simulation time. It is noticeable that the first few seconds are affected by transients, so the reported graphs focus on the last oscillations.

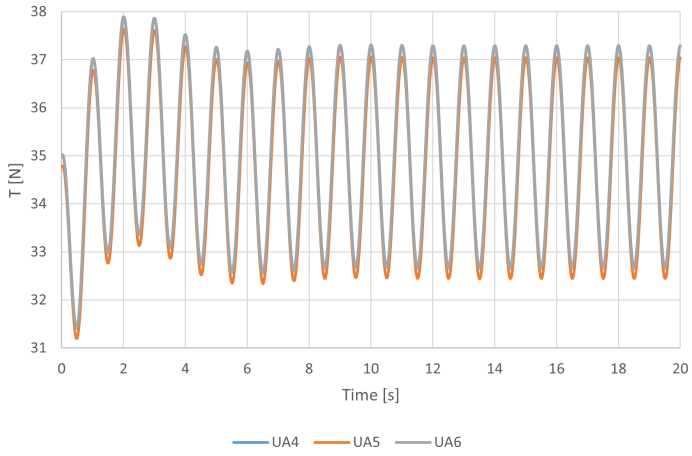

Figure 4.9: Thrust of case 2.5 for the whole simulation time

Surge case 2.5

This initial unsteady case simulates a surge motion of $\Theta = 0.035$ m and $f = 1$ Hz, with the turbine rotating at 4 Hz (240 rpm). In Figure 4.10, where one motion period corresponds to one second, the thrust and torque results obtained from different dynamic stall models are presented. UA5 is visibly lower than the other two, which essentially overlap each other.

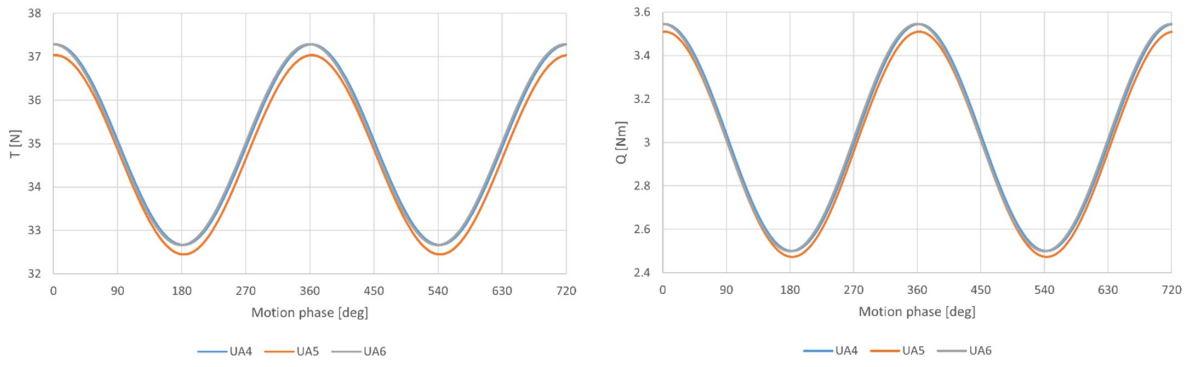

Figure 4.10: Thrust and torque of case 2.5 for different models

This observation is confirmed by the data in Table 4.11, where UA4 and UA6 have very close values, while UA5 has an approximately -0.7% deviation from them in thrust and about -1% in torque. Nonetheless, the differences are quite small, with all three models agreeing with the results from OC6, although they are still lower than the Ex1 values. Lastly, the power produced by the turbine remains relatively consistent across the three models. For example, UA4 oscillates between a maximum of 89.11 W and a minimum of 62.85 W, generating a ± 17% fluctuation around the mean of 75.87 W. This last value corresponds to the steady wind power recorded in case 1.1. Additionally, the "delta" rows refer to the difference between the maximum and minimum values (i.e. peak-to-peak amplitude), which in this case is 26.26 W.

Table 4.11: Case 2.5 characteristics

		UAMod		
Output		**4**	**5**	**6**
T [N]	**mean**	34.99	34.75	34.99
	max	37.29	37.04	37.29
	min	32.67	32.45	32.66
	delta	4.62	4.59	4.63
Q [Nm]	**mean**	3.02	2.99	3.02
	max	3.55	3.51	3.55
	min	2.50	2.47	2.50
	delta	1.04	1.04	1.05

Output		4	5	6
P [W]	**mean**	75.87	75.09	75.87
	max	89.11	88.23	89.13
	min	62.85	62.17	62.83
	delta	26.26	26.06	26.30

Another simulation was run utilizing the DBEMT settings without the correction for aerodynamic coefficients to understand their influence. The graphs depicted in Figure 4.11 show this configuration through the black, dotted "DBEM" lines, comparing it to the UA4 and UA6 models. As the UA5 exhibited noticeable peak asymmetries, previously in the 5MW analysis, it is less interesting in the end. Graphically, very little differences are noticeable, while the values reported in Table 4.12 reveal that the DBEM ones share the same peak-to-peak amplitude but are shifted down by a limited -0.2% with respect to the UA results.

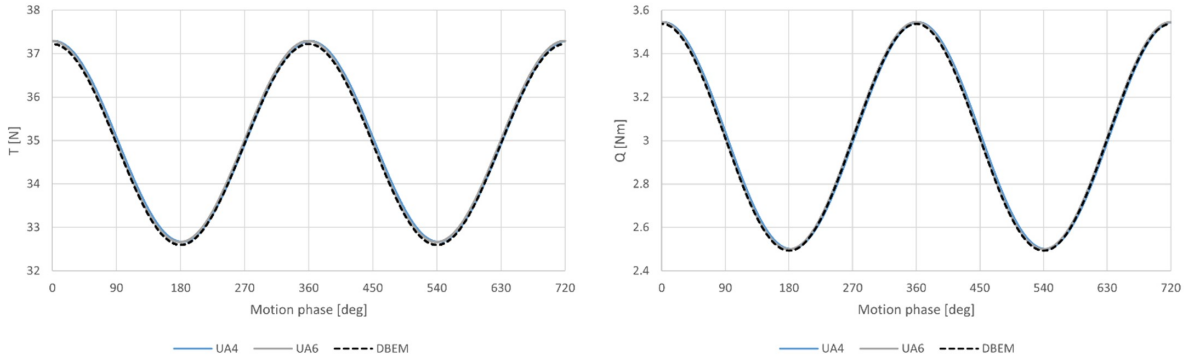

Figure 4.11: Thrust and torque of case 2.5 with DBEM

Output		DBEM	Output		DBEM	Output		DBEM
T [N]	**mean**	34.92	**Q [Nm]**	**mean**	3.01	**P [W]**	**mean**	75.68
	max	37.22		**max**	3.54		**max**	88.92
	min	32.60		**min**	2.49		**min**	62.65
	delta	4.62		**delta**	1.05		**delta**	26.27

Table 4.12: Case 2.5 DBEM characteristics

Pitch case 3.5

The pitch platform motion case 3.5 shares the same frequency as case 2.5 but $\Theta = 1.4$ deg. The yielded results closely resemble those of the prior simulation, as this case is designed

to have an equivalent wind variation. As shown in Figure 4.12, the same disagreement of UA5 reemerges, reflecting the same -0.7% and -1% lower values, which are obtained by looking at Table 4.13.

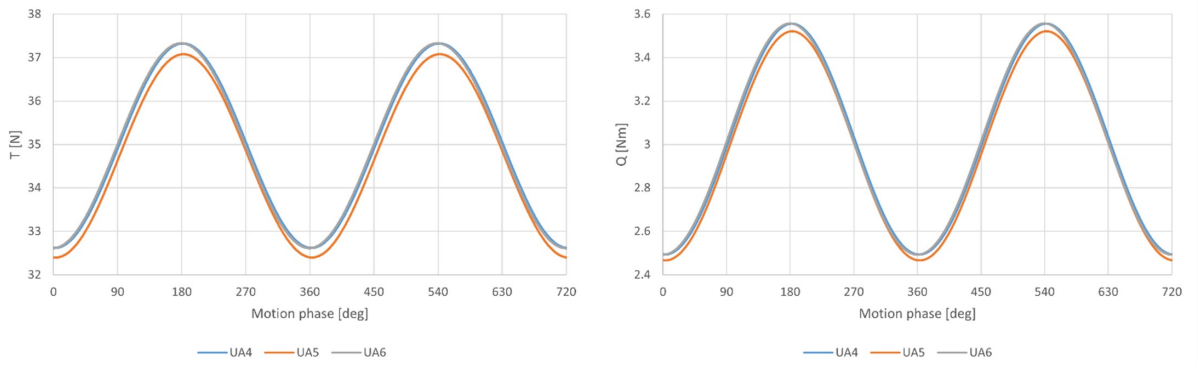

Figure 4.12: Thrust and torque of case 3.5 for different models

Referring to the power in the table, the mean is quite similar to the one from the surge and steady cases. Furthermore, the peak-to-peak amplitude, reported as delta, surpasses those of the surge cases, with UA6 reaching 26.75 W, 1.7% higher than the UA6 surge case. This result notably diverges from the Ex2 value depicted in the figures within the OC6 report.

Table 4.13: Case 3.5 characteristics

		UAMod		
Output		**4**	**5**	**6**
T [N]	**mean**	34.98	34.74	34.98
	max	37.33	37.08	37.33
	min	32.62	32.40	32.61
	delta	4.71	4.68	4.72
Q [Nm]	**mean**	3.02	2.99	3.02
	max	3.56	3.52	3.56
	min	2.49	2.47	2.49
	delta	1.06	1.05	1.06
P [W]	**mean**	75.85	75.07	75.85
	max	89.37	88.49	89.40
	min	62.67	61.99	62.65
	delta	26.70	26.50	26.75

Figure 4.13 and Table 4.14 detail the comparison with the DBEMT simulation, similar to preceding analysis. The difference is still very small, with the DBEM results exhibiting a slight shift to lower values.

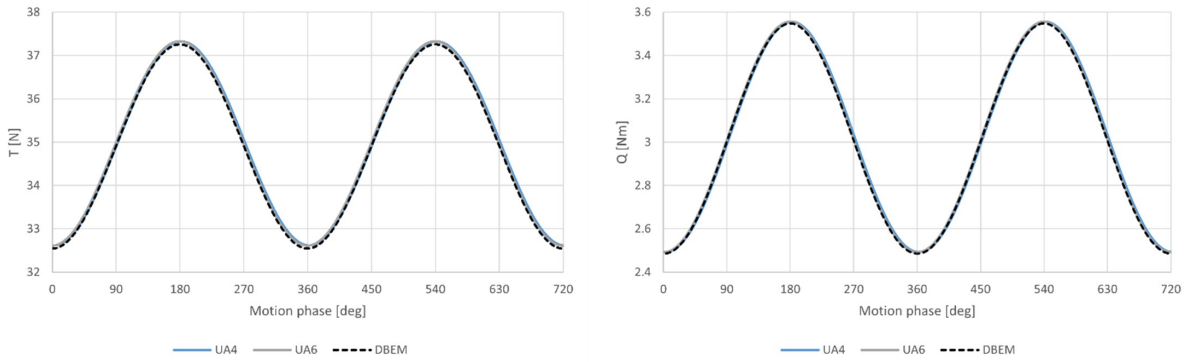

Figure 4.13: Thrust and torque of case 3.5 with DBEM

Output		DBEM	Output		DBEM	Output		DBEM
T [N]	**mean**	34.91	**Q [Nm]**	**mean**	3.01	**P [W]**	**mean**	75.66
	max	37.26		**max**	3.55		**max**	89.18
	min	32.55		**min**	2.49		**min**	62.47
	delta	4.71		**delta**	1.06		**delta**	26.71

Table 4.14: Case 3.5 DBEM characteristics

Surge case 2.12

This surge case has a more important platform motion, characterized by $\Theta = 0.08$ m and $f = 2$ Hz, twice that of the previous cases. As a result, the movement is more rapid, and one period represented in the graphs lasts only half a second.
Figure 4.14 shows the familiar, regular trend, although the graph and the values in Table 4.15 illustrate the greater variations due to the intensified motion. In fact, the peak-to-peak amplitudes are more than 3 times the ones from case 2.5. The power, for example, which variation is important for the electrical components of the turbine, reaches a delta of 112.89 W in UA4, contrasting with the 26.26 W value of the aforementioned case.
Furthermore, the mean power (and torque) is higher than both the steady and case 2.5 ones, however, the thrust is lower, signifying an increased tangential loading of the blade.

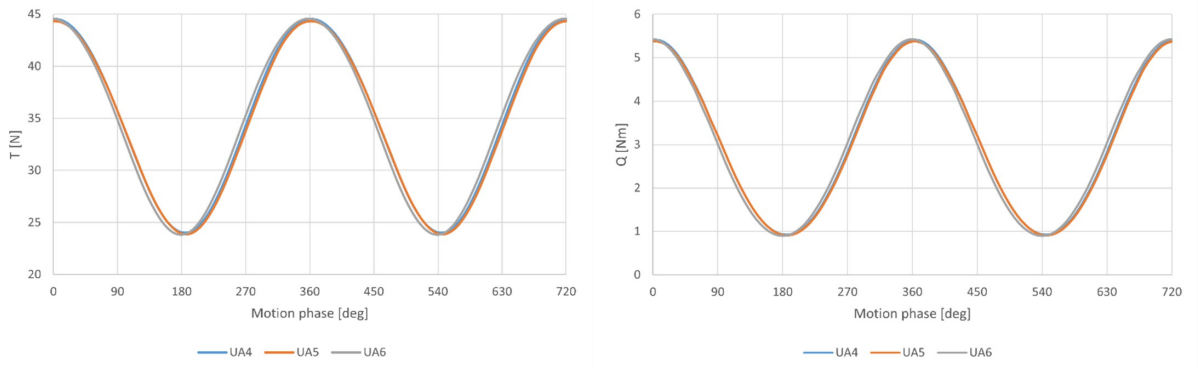

Figure 4.14: Thrust and torque of case 2.12 for different models

When assessing the differences between the models, UA5 now exhibits closer alignment with the others. This behavior is similar to the one encountered in Chapter 3 on the 5MW turbine, visually represented in Figure 3.2. At higher frequencies and amplitudes, the different dynamic stall models agree more than at the lower ones. Minor divergences persist in both the thrust and torque.

Table 4.15: Case 2.12 characteristics

		UAMod		
Output		**4**	**5**	**6**
T [N]	**mean**	34.67	34.45	34.63
	max	44.55	44.33	44.57
	min	24.02	23.87	23.82
	delta	20.53	20.46	20.75
Q [Nm]	**mean**	3.09	3.06	3.09
	max	5.42	5.38	5.43
	min	0.92	0.91	0.90
	delta	4.49	4.47	4.53
P [W]	**mean**	77.76	77.03	77.68
	max	136.10	135.10	136.40
	min	23.21	22.88	22.60
	delta	112.89	112.22	113.80

The following figure and table report the DBEM simulation, with observations similar to the previous cases.

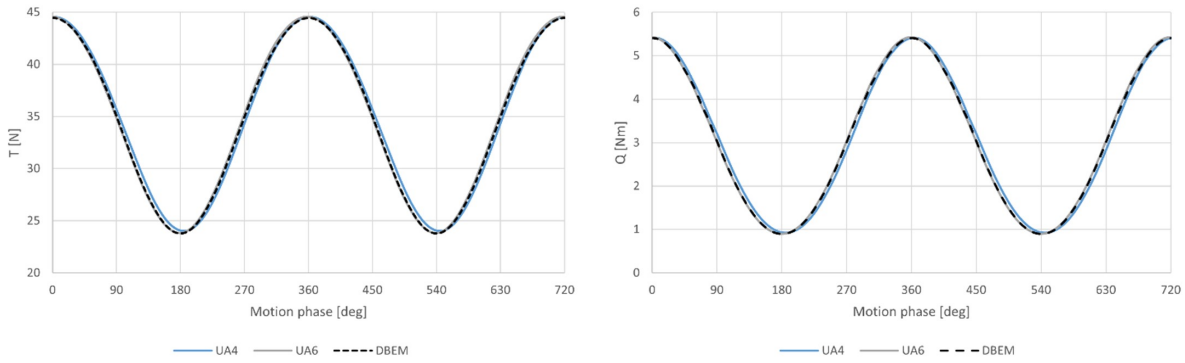

Figure 4.15: Thrust and torque of case 2.12 with DBEM

Output		DBEM	Output		DBEM	Output		DBEM
T [N]	**mean**	34.55	**Q [Nm]**	**mean**	3.08	**P [W]**	**mean**	77.42
	max	44.45		**max**	5.41		**max**	135.90
	min	23.78		**min**	0.90		**min**	22.52
	delta	20.67		**delta**	4.51		**delta**	113.38

Table 4.16: Case 2.12 DBEM characteristics

Normalized loads and phase shift

An additional analysis can be conducted concerning the different *UAMod* options by calculating the normalized thrust and torque in relation to the peak-to-peak amplitude of the motion, along with their phase shift with respect to the platform motion.
The first one considers the peak-to-peak amplitudes in meters, so it is 0.035 m for case 2.5 and 0.08 m for 2.12. While to convert the 1.4 deg to the correct unit, the equivalent motion amplitude at the hub can be calculated using the formula: (Hub height) * sin(1.4). Given that the hub height corresponds to 1.464 m, the obtained value is 0.0357 m. By dividing the delta of the previous tables by these newly calculated values, the following Table 4.17 is obtained.

	THRUST [N/m]			**TORQUE [Nm/m]**		
	Case			**Case**		
UAMod	**2.5**	**3.5**	**2.12**	**2.5**	**3.5**	**2.12**
4	132	131.68	256.63	29.86	29.69	56.14
5	131.14	130.84	255.75	29.63	29.47	55.81
6	132.29	131.96	259.38	29.89	29.75	56.6

Table 4.17: Normalized thrust and torque peak-to-peak values

The results reinforce the similarities between the dynamic stall models observed earlier. Additionally, cases 2.5 and 3.5 demonstrate similar normalized result as they reproduce comparable conditions. Conversely, case 2.12 has greater values, due to the higher frequency of its imposed motion. The DBEM simulations are not included in this analysis since they previously showed the same peak-to-peak amplitudes to the other models.
The phase shift was determined by comparing the "0" points of the oscillations, referencing the visualization of the parameter in Figure 4.16, taken from the OC6 report.

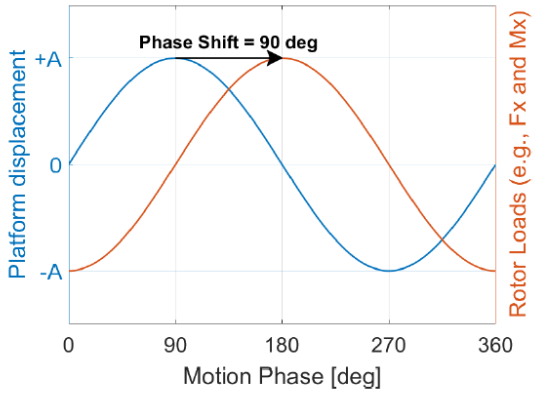

Figure 4.16: Phase shift between motion and loads as visualized in [6]

First, the outputs were filtered using a Matlab low-pass filter function with a cut-out frequency of 1.5 Hz for the cases 2.5 and 3.5 and 2.5 Hz for case 2.12. The obtained waves were then matched to their mean to identify the closest value to them and its time instant. These found time points were finally compared to the corresponding "mean point" time instant of the platform motion input, converting the time to the phase shift in degrees. Because of the high frequencies, a single time step corresponds to a relatively high phase shift increment, thereby introducing a degree of uncertainty into the results. Table 4.18 reports the phase shift of UA4 and UA6, as their previous graphs indicated some notable distinctions.

	THRUST [deg]			**TORQUE [deg]**		
	Case			**Case**		
UAMod	**2.5**	**3.5**	**2.12**	**2.5**	**3.5**	**2.12**
4	91.8	91.8	91.44	92.88	93.24	96.48
6	89.28	89.28	86.4	90.36	90.36	91.44

Table 4.18: Phase shift of thrust and torque relative to the platform motion

The table shows again the agreement between cases 2.5 and 3.5, except for the torque in UA4, where a one time-step difference can be observed. UA6 is overall closer to the expected phase shift of 90 deg for both thrust and torque, while UA4 has a greater lag. Furthermore, it can be observed that case 2.12 shows more distant values from 90 deg in both models (UA5, which is not reported, showed an overall worse lag than UA4). Lastly, torque, as confirmed also by the median simulation results of the OC6 report, displays a slightly higher phase shift, even greater in case 2.12.

Surge case 2.17 with variable blade pitch

The last verification case 2.17, stems from case 2.12 by implementing the collective blade pitch routine of Figure 4.7. Figure 4.17 illustrates the effect of this addition on the C_l and AoA of the 10th node (62.8% of the blade span) of blade 1: the left side depicts case 2.12, while the right shows case 2.17. The introduction of variation of pitch leads to a reduction in the peak-to-peak amplitude of the AoA, consequently decreasing the one of the C_l. This variation becomes evident in the following Figure 4.18.

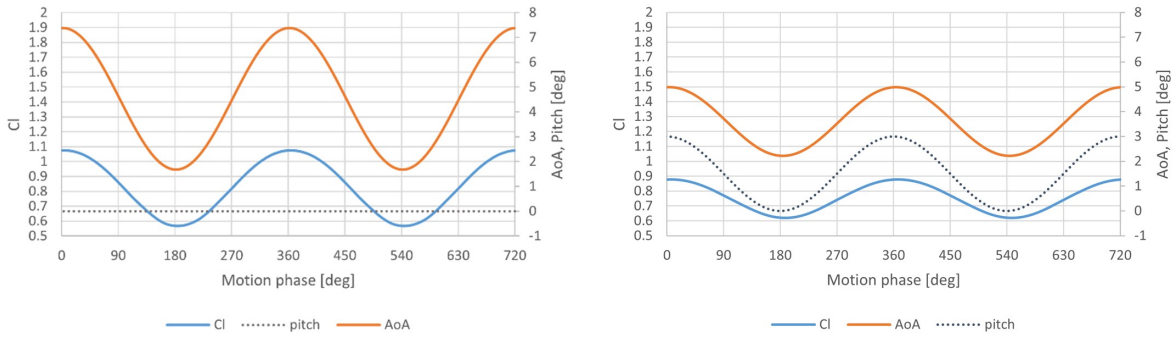

Figure 4.17: C_l and AoA variation in case 2.12 vs 2.17

Here, the thrust and torque of case 2.17 for the UA4 and UA6 models are plotted alongside the UA4 results of case 2.12 (depicted in yellow) and the blade pitch, indicated by the dotted line. The reduction in C_l at the maximum greatly affects the thrust, which decreases from 44.55 N to 37.66 N (UA4), with a percentage change of -15.5%. Conversely, the minimum presents a smaller 7.3% increase. This peak-to-peak amplitude of the thrust agrees with the results of the OC6 report, which also highlights the importance of implementing the dynamic inflow model in presence of blade pitch actuation, as its steps or sudden changes are one of the known causes of the phenomenon. The peak-to-peak amplitude reduction is also evident in the torque and power, albeit with less magnitude, nonetheless, the delta of the power is minimized in this case, measuring 93.63 W as opposed to the 112.89 W of case 2.12. Lastly, the mean values are realigned with the steady

ones of case 1.1.

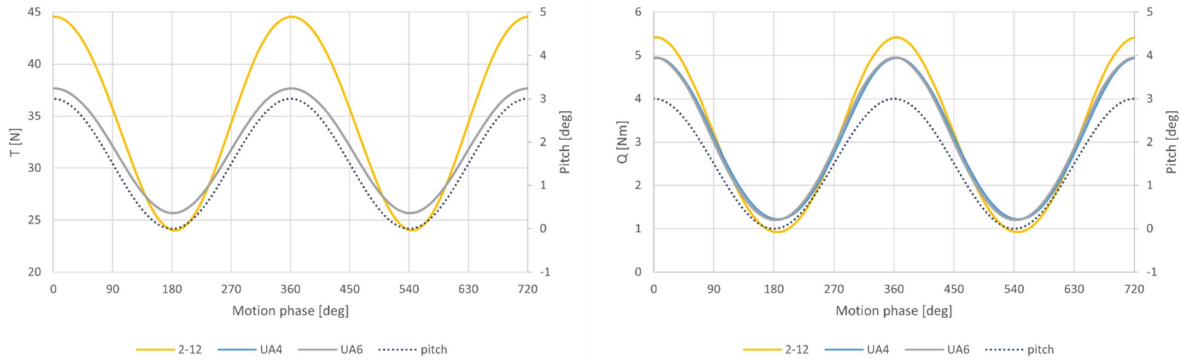

Figure 4.18: Thrust and torque of case 2.17 for different models

The DBEM simulation follows a pattern similar to the that of case 2.12 and it is reported in the Table 4.19 below. This blade pitch variation solution has demonstrated a successful method in mitigating the loading oscillations on the machine, which reached extreme values in the case before.

Table 4.19: Case 2.17 characteristics

		UAMod		
Output		**4**	**6**	**DBEM**
T [N]	**mean**	31.82	31.80	31.73
	max	37.66	37.66	37.56
	min	25.77	25.67	25.63
	delta	11.89	11.99	11.93
Q [Nm]	**mean**	3.01	3.01	3.00
	max	4.94	4.95	4.94
	min	1.22	1.20	1.20
	delta	3.73	3.75	3.74
P [W]	**mean**	75.63	75.59	75.35
	max	124.27	124.48	124.09
	min	30.65	30.18	30.10
	delta	93.63	94.30	93.99

5 | Conclusions and future developments

This thesis aimed to investigate the feasibility and the reliability of utilizing the OpenFAST models for simulating the load response of FOWTs subjected to platform motions. The analysis employed a BEMT approach, expanded to account for the unsteady aspects of the FOWT configurations. To enhance accuracy, the dynamic wake effects have been included in DBEMT calculations, complemented by dynamic stall models developed by B-L and Øye. These methodologies have also been compared against CFD results of the standardized NREL offshore 5MW baseline wind turbine. Moreover, the OpenFAST tool has been used to simulate the scaled turbine model of the UNAFLOW project, allowing for the validation of output accuracy through a comprehensive comparison with experimental campaigns.

The first analysis has focused on the 5MW turbine and compares new results with a wide set of previous calculations. The initial replication of one extreme pitching motion case, with $\Theta = 4$ deg and $f = 0.2$ Hz, has highlighted the updates made to the OpenFAST code. The Øye model had been corrected, leading to improved agreement among the available dynamic stall options. This has also showcased the advantage of this tool's potential for continuous improvement across its versions.

A second, similar analysis has focused on additional pitch motion scenarios with the 5MW turbine, created by the combination of different frequency and amplitude values. This has produced a wide range to study the behavior of the models. A comparison with an OpenFAST dynamic stall model from an earlier version of the tool has revealed an overall consistent trend among the options, characterized by predominantly sinusoidal and symmetric responses in all cases. However, the updated models have showed two forms of disagreements with the former ones. Firstly, cases with lower platform loads have exhibited higher mean, maximum, and minimum values by a small margin. Secondly, in the highest load case of $f = 0.1$ Hz and $\Theta = 4$ deg, the updated models have demonstrated closer trends but have encountered issues in the maximum region. Disagreements have risen in the peak values and shape, resulting in differences of about $\pm$ 1% in the

numerical values and partial loss of the symmetry with peaks showing before expected maximum, probably due to numerical problems. These issues are especially evident in the B-L type calculations. This observations have been corroborated through comparison with CFD results. The value shift has again been more pronounced in smaller motion cases, while the CFD peak has been notably higher than those of the OpenFAST simulations. Upon investigating the dynamic influences on the results, it has been revealed that at the minimum load point of a motion cycle, only the steady BEMT model has displayed differences. These discrepancies have been attributed to the AoA, where deviations between very low angles are present. Steady BEMT simulations diverged from all other models that included dynamic correction. Conversely, the dynamic models have captured the phenomena with the consistent precision and have showed the same AoA trend. Furthermore, moving to the maximum point, differences have emerged in the values corrected by different dynamic stall models for the C_l, and, to a lesser extent, the C_d. These differences were concentrated towards the root of the blade, an area particularly susceptible to flow detachment. This last observation also explains the greater differences in the values of the thrust force, which is more influenced by the root compared to the power.

This work has expanded to the implementation of the scaled turbine of the UNAFLOW experiment in the tool. Furthermore, this investigation concerned the dynamic stall models listed before and DBEMT calculations without them. This analysis required the modification of the input files first; then, relevant cases from the experimental campaign have been selected to be able to simulate different DoFs: surge, pitch, and blade pitch regulation. The cases included steady wind scenarios that have been used as a base case for the configurations. These first results have aligned with the other BEMT values obtained during the OC6 project on the same campaign, confirming the validity of this approach. However, they have also revealed a certain distance from the experimental results, a trend that has persisted across all the other cases. Following this, analogous pitch and surge cases have been simulated, yielding consistent results from all the dynamic models. The platform motion has induced sinusoidal responses with an important peak-to-peak amplitude of about 26 W. Considering the average value of about 75 W, an oscillation of $\pm$ 17% has been observed. Specifically, the B-L 5-states model has presented lower values. However, this model has not been further investigated as its issues in the prior simulations deemed it less interesting for this work. Case 2.12 has exhibited smaller differences among the results compared to the other cases, nonetheless, the significant platform motion has magnified the oscillation of the aerodynamic loads, resulting in a peak-to-peak power amplitude of around 112 W, more than three times that of the previously mentioned cases. Out of these three cases, normalized loads to the amplitude of the motion and phase shifts

were calculated. Normalized loads have exhibited a correlation with the frequency of the motion, while the phase shifts have predominantly shown values around 90 deg. The B-L 4-states model has shown a slight delay compared to the Øye one. This effect has been noted to be greater for the torque and to increase at higher frequencies, coherently with the trends shown in the OC6 report. Lastly, the implementation of collective blade pitch regulation has introduced a successful method for reducing the oscillations of the loads on the turbine. The AoA variation from case 2.12 has led to a consequent reduction in C_l, particularly effective in diminishing the peak values. The previous peak-to-peak amplitude of the power has been decreased to 94 W.

These simulations have demonstrated the reliability of OpenFAST results, which have aligned satisfactorily with CFD and experiments.

In future developments, due to the continuous improvement of the tool, OpenFAST analyses may be extended to include updated or newer models, aiming to identify the best solution for FOWT configurations. Additionally, the simulations in this work were limited to the essential calculations, leaving room to include other modules and inputs to better replicate real-life conditions. Among these integrations, it may be interesting to implement more realistic control strategies, as the open-circuit blade pitch regulation was quite successful, albeit simplified.

Bibliography

[1] Openfast-github. URL https://github.com/OpenFAST.

[2] Webplotdigitizer. URL https://apps.automeris.io/wpd/.

[3] Openfast 3.4.1 documentation, api changes between versions, 2023. URL https://openfast.readthedocs.io/en/v3.4.1/source/user/api_change.html.

[4] Openfast 3.4.1 documentation, 2023. URL https://openfast.readthedocs.io/en/v3.4.1/source/this_doc.html.

[5] I. Bayati, M. Belloli, L. Bernini, D. M. Boldrin, K. Boorsma, M. Caboni, M. Cormier, R. Mikkelsen, T. Lutz, and A. Zasso. UNAFLOW project: UNsteady Aerodynamics of FLOating Wind turbines. *Journal of Physics: Conf. Series*, 2018.

[6] R. Bergua and et al. OC6 project Phase III: validation of the aerodynamic loading on a wind turbine rotor undergoing large motion caused by a floating support structure. *Wind Energ. Sci.*, 8:465–485, 2023.

[7] E. Branlard. *Wind Turbine Aerodynamics and Vorticity-Based Methods, Fundamentals and Recent Applications*. Springer, 2017.

[8] E. Branlard, B. Jonkman, G. R. Pirrung, K. Dixon, and J. Jonkman. Dynamic inflow and unsteady aerodynamics models for modal and stability analyses in openfast. *J, Phys.: Conf. Ser.*, 2265, 2022.

[9] S. Butterfield, W. Musial, J. Jonkman, and P. Sclavounos. Engineering challenges for floating offshore wind turbines. *NREL Conference Paper*, 2007.

[10] Enel. L'eolico in italia: quanta energia si produce e dove, 2023. URL https://www.enelgreenpower.com/it/learning-hub/energie-rinnovabili/energia-eolica/energia-eolica-italia.

[11] European Council. Fit for 55, 2023. URL https://www.consilium.europa.eu/en/policies/green-deal/fit-for-55-the-eu-plan-for-a-green-transition/.

[12] European Parliament. Climate change in europe: facts and figures,

2023. URL https://www.europarl.europa.eu/news/en/headlines/society/20180703STO07123/climate-change-in-europe-facts-and-figures.

[13] M. H. Hansen, M. Gaunaa, and H. A. Madsen. A beddoes-leishman type dynamic stall model in state-space and indicial formulations. *ø-R-1354(EN)*, 2004.

[14] M. O. L. Hansen. *Aerodynamics of wind turbines*. Earthscan, 2 edition, 2008. ISBN 978-1-84407-438-9.

[15] B. Jonkman and J. Jonkman. Fast v8.16.00a-bjj. *NREL*, 2016.

[16] J. Jonkman. Openfast: An open-source tool for wind turbine physics-based engineering modeling, 2022. URL https://drive.google.com/file/d/1bD5a6rRg6cCKht9Ar8AFJQ8YrI4-wsFe/view.

[17] J. Jonkman, S. Butterfield, W. Musial, and G. Scott. Definition of a 5-mw reference wind turbine for offshore system development. *NREL Technical Report*, 2009.

[18] J. M. Jonkman and M. L. B. Jr. Fast user's guide. *NREL Technical Report*, 2005.

[19] NREL Forum. Aerodyn dynamic stall model, 2021. URL https://forums.nrel.gov/t/aerodyn-dynamic-stall-model/2568.

[20] A. Ortolani. High- and low-fidelity calculations of a floating off-shore wind turbine under pitching motion. Master's thesis, Politecnico di Milano, 2019.

[21] A. Ortolani, G. Persico, J. Drofelnik, A. Jackson, and M. Campobasso. Cross-comparative analysis of loads and power of pitching floating offshore wind turbine rotors using frequency-domain navier-stokes cfd and blade element momentum theory. *Journal of Physics: Conf. Series* , 2020.

[22] A. Robertson, R. Bergua, A. Fontanella, and J. Jonkman. OC6 Phase III Definition Document. 2022.

[23] B. Skaare, F. G. Nielsen, T. D. Hanson, R. Yttervik, O. Havmøller, and A. Rekdal. Analysis of measurements and simulations from the hywind demo floating wind turbine. *Wind Energ.*, 18:1105–1122, 2015.

[24] Wind Europe. Floating offshore wind vision statement, 2017. URL https://windeurope.org/wp-content/uploads/files/about-wind/reports/Floating-offshore-statement.pdf.

[25] Wind Europe. Wind energy today, 2023. URL https://windeurope.org/about-wind/wind-energy-today/.

[26] A. Zappulla. An investigation of unsteady aerodynamic models for load and performance predictions of floating off-shore wind turbine. Master's thesis, Politecnico di Milano, 2021.

A | Appendix A

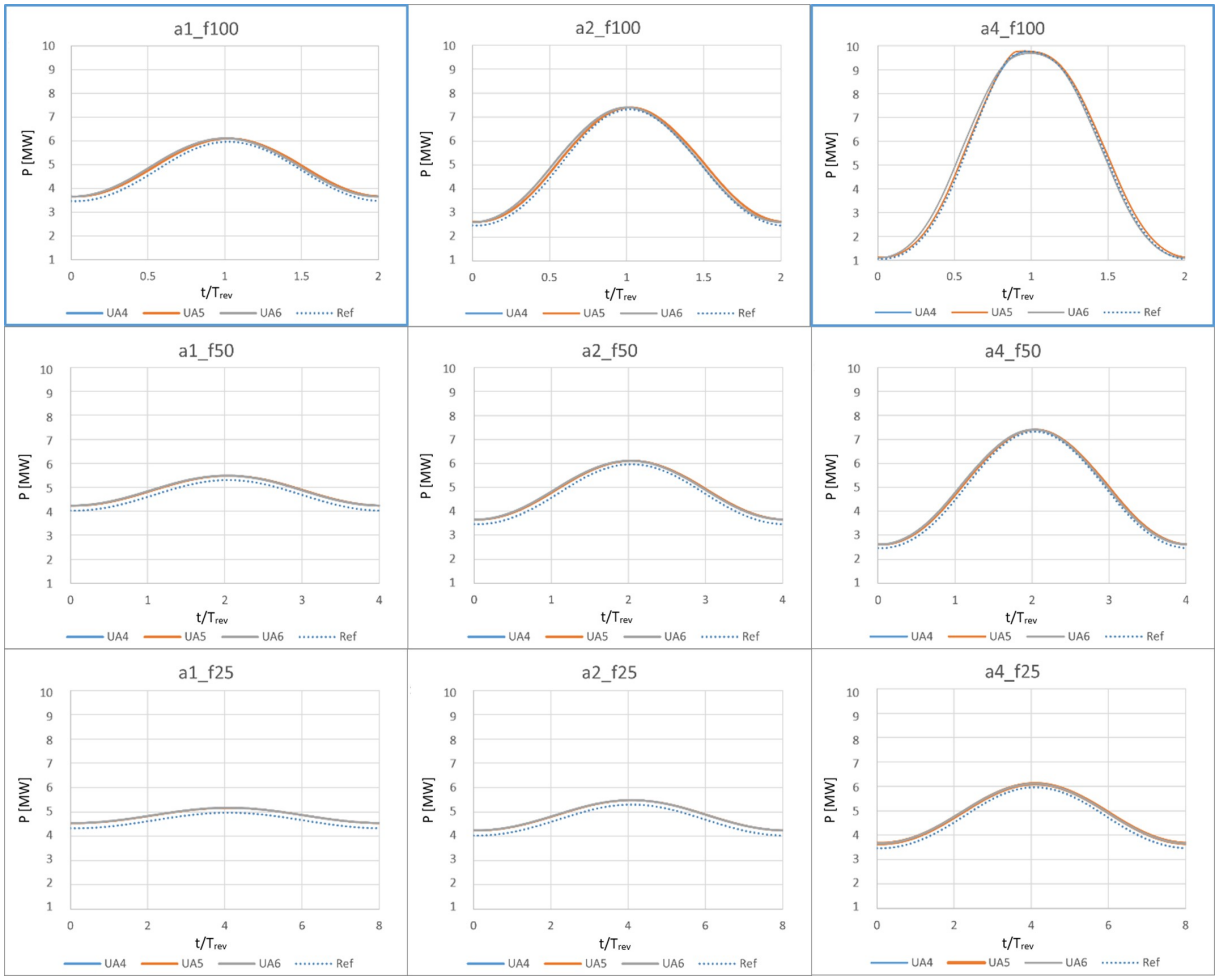

Figure A.1: Power of the 5MW nine simulated cases

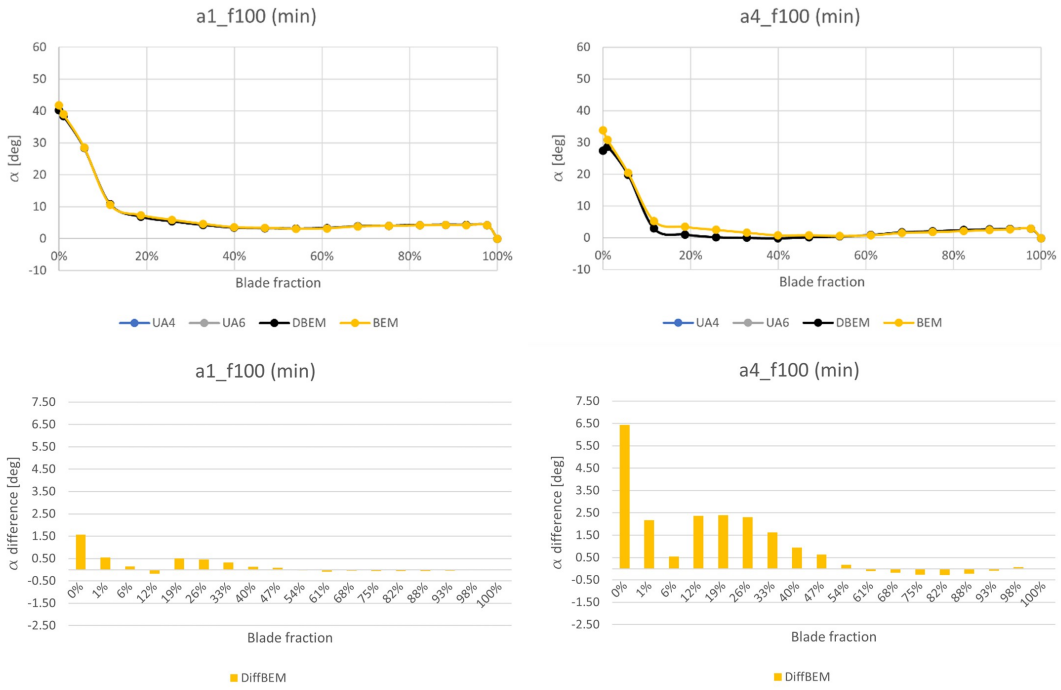

Figure A.2: Minimum point AoA for the two cases. blade 2

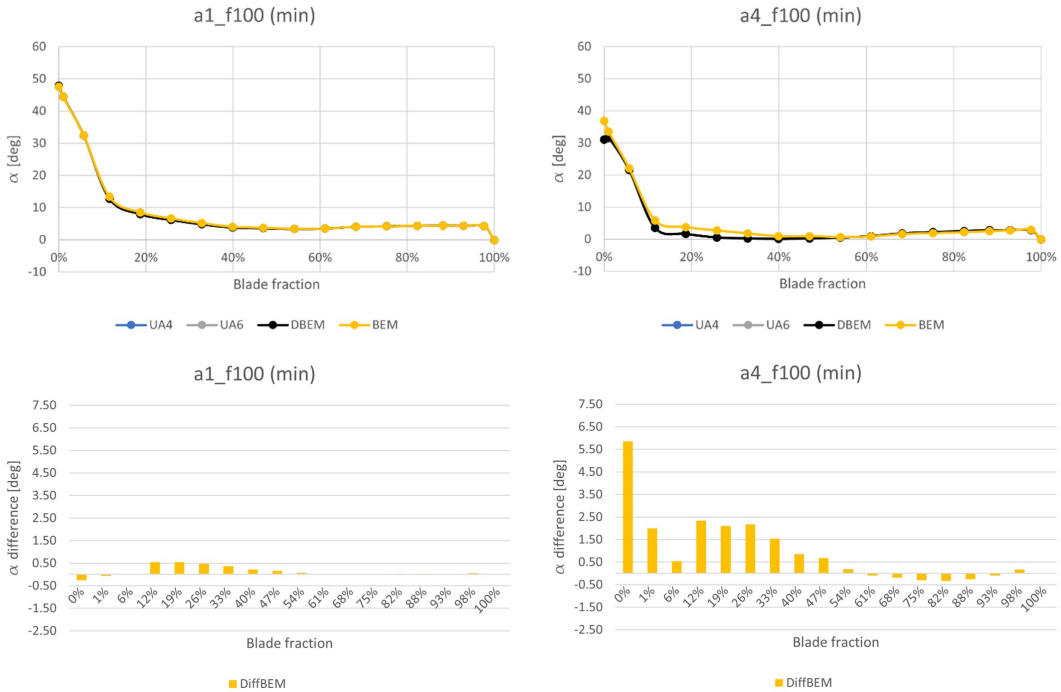

Figure A.3: Minimum point AoA for the two cases. blade 3

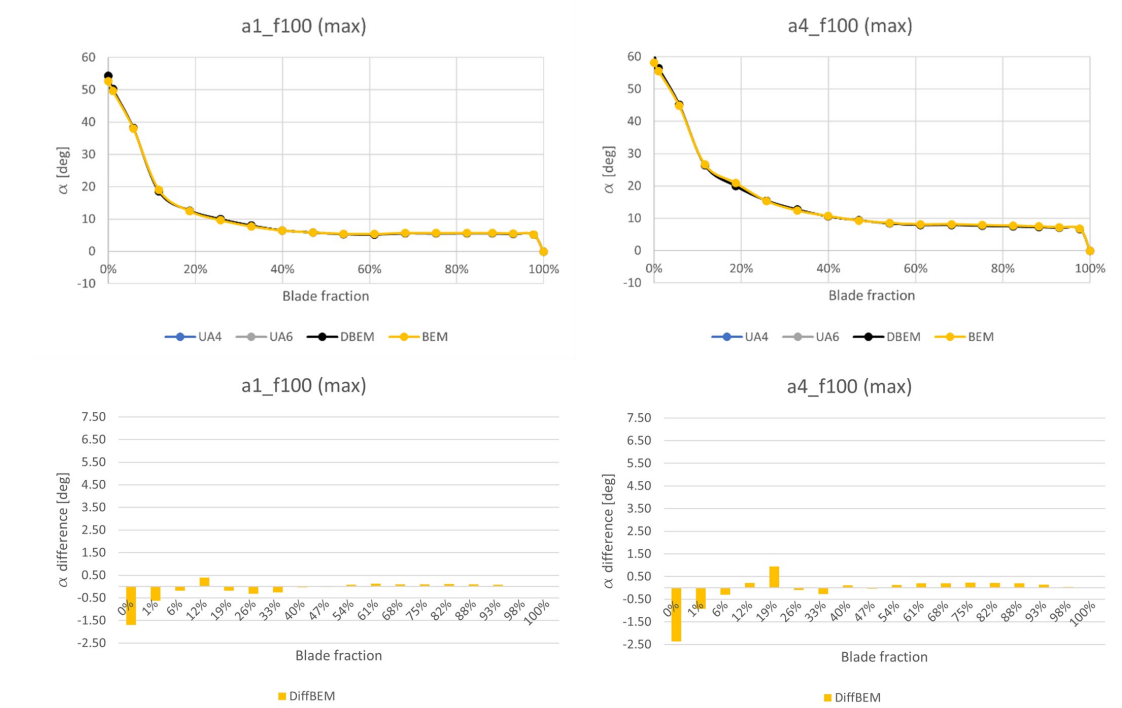

Figure A.4: Maximum point AoA for the two cases. blade 3

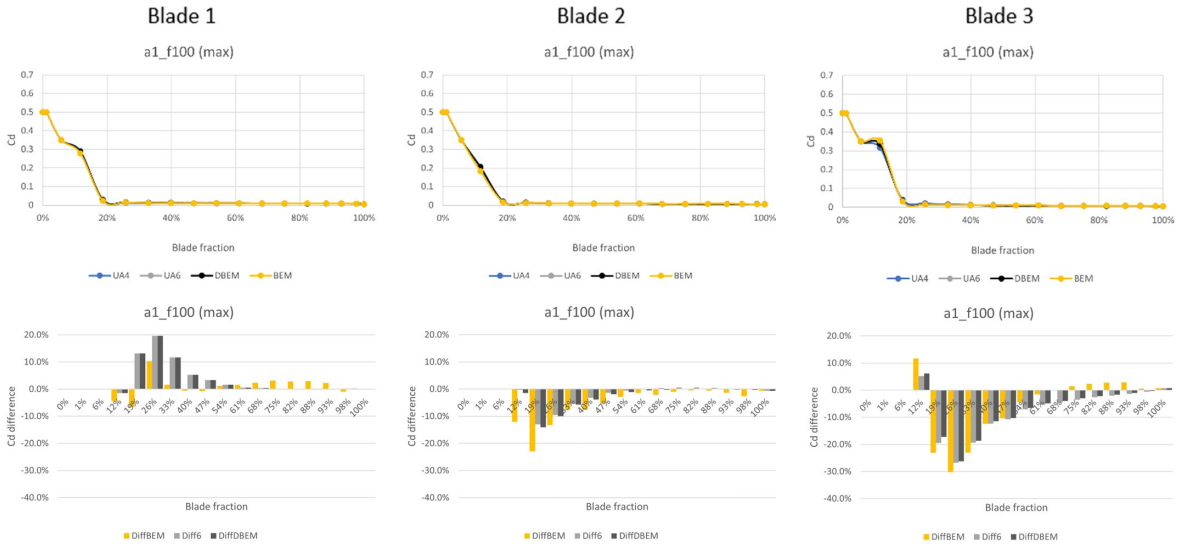

Figure A.5: Maximum point C_d of the three blades for $\Theta = 1$ deg